



ALMA MATER STUDIORUM
UNIVERSITÀ DI BOLOGNA

ARCHIVIO ISTITUZIONALE
DELLA RICERCA

Alma Mater Studiorum Università di Bologna Archivio istituzionale della ricerca

Simulation of observed temperature field below a building in Bologna, Italy

This is the final peer-reviewed author's accepted manuscript (postprint) of the following publication:

Published Version:

Focaccia, S., Barbaresi, A., Tinti, F. (2020). Simulation of observed temperature field below a building in Bologna, Italy. ENVIRONMENTAL GEOTECHNICS, 7(4), 295-305 [10.1680/jenge.17.00105].

Availability:

This version is available at: <https://hdl.handle.net/11585/651692> since: 2024-07-18

Published:

DOI: <http://doi.org/10.1680/jenge.17.00105>

Terms of use:

Some rights reserved. The terms and conditions for the reuse of this version of the manuscript are specified in the publishing policy. For all terms of use and more information see the publisher's website.

This item was downloaded from IRIS Università di Bologna (<https://cris.unibo.it/>).
When citing, please refer to the published version.

(Article begins on next page)

1 Simulation of observed 2 temperature field below a building

3 Author 1

- 4 • Eng. PhD. Sara Focaccia
- 5 • SERENGEO srl, Bologna, Italy
- 6 • 0000-0002-1293-4914

7 Author 2

- 8 • Eng. PhD. Alberto Barbaresi
- 9 • Department of Agricultural Sciences, University of Bologna, Bologna, Italy
- 10 • 0000-0003-1341-984X

11 Author 3

- 12 • Eng. PhD. Francesco Tinti*
- 13 • Department of Civil, Chemical, Environmental and Materials Engineering, University of
14 Bologna, Bologna, Italy
- 15 • 0000-0002-6750-9368

16 Paper submitted: 14/12/2017.

17 Paper revised: 15/05/2018.

18 *Corresponding Author: Francesco Tinti.

19 Department of Civil, Chemical, Environmental and Materials Engineering, University of Bologna,
20 via Terracini 28, 40100 Bologna, Italy.

21 E-mail: francesco.tinti@unibo.it

22 Phone: +390512090477

23
24
25

1
2
3
4
5
6
7
8
9
10
11
12
13
14
15
16
17
18
19
20
21
22
23
24
25
26
27
28
29
30
31
32
33
34
35
36
37
38
39
40
41
42
43
44
45
46
47
48
49
50
51
52
53
54
55
56
57
58
59
60
61
62
63
64
65

26 Abstract

27 Urban settlements, whether single buildings or apartment blocks, influence near-surface ground
28 temperatures. Heat transfer by buildings to the ground must therefore be considered when
29 designing both vertical probes and energy geostructures in urban areas. However, assessment
30 of ground temperature variability in urban areas is still uncommon for shallow geothermal
31 energy purposes, the standard temperature gradient based on climatic conditions usually being
32 employed during the design phase. Yet precise assessment of the heat transfer between
33 buildings, infrastructures and the underground could improve the planning of geothermal
34 systems.

35 This work presents a numerical simulation of a finite-element model of heat transfer to the
36 underground due to both a single building and climate conditions with the aim of reproducing
37 the temperature waves at each depth. An isolated building was chosen since it allowed exact
38 quantification of its influence on the ground temperature without external interferences. For this
39 purpose, different boundary and initial conditions were applied to the ground thermal model and
40 results were compared with historical data recorded over several years. The idea proposed in
41 the paper for a single building can be considered as the baseline for further ground temperature
42 assessment of wider urban settlements.

43 Keywords

44 Ground temperature; Shallow geothermal energy; Finite-element modelling.

45 List of notation

46 T_g is the varying space-time underground temperature,

47 T_{me} is the average annual surface temperature,

48 $T_{building}$ is the temperature inside the building,

49 T_{cellar} is the temperature inside the cellar,

50 A_e is the annual surface wave amplitude,

51 t_{T0} is the time at minimum temperature,

52 α is the equivalent thermal diffusivity,

53 λ is the equivalent thermal conductivity,

54 ρ is the density,

1
2
3
4
5
6
7
8
9
10
11
12
13
14
15
16
17
18
19
20
21
22
23
24
25
26
27
28
29
30
31
32
33
34
35
36
37
38
39
40
41
42
43
44
45
46
47
48
49
50
51
52
53
54
55
56
57
58
59
60
61
62
63
64
65

55 C is the heat capacity,

56 ρC is the volumetric heat capacity.

57

1 58 **1. Introduction**

2
3 59 The subsurface temperature gradient, or geothermal gradient, depends mainly on endogenous
4
5 60 geothermal heat flow (Cermak and Rybach, 1979). However, in shallow layers, its contribution is
6
7 61 limited, and subsoil temperature follows climate seasonality, which is damped on account of
8
9 62 ground thermal insulation that varies with geological and hydrogeological conditions (Kusuda
10
11 63 and Achenbach, 1965). As a result, ground temperatures at very shallow depths change in
12
13 64 space - vertically, because of climate wave dampening, and horizontally, due to the variation of
14
15 65 geological and hydrogeological conditions - and time, following the ambient temperature wave
16
17 66 (Baggs, 1985). It follows that at a certain depth and thickness, depending on local conditions, a
18
19 67 ground layer, or so-called neutral zone, will exist where temperature variations in space and
20
21 68 time become nil before geothermal heat flow resumes, with the resulting geothermal gradient
22
23 69 (Pouloupatis et al., 2011).

24
25 70 Shallow layer ground temperature should also take into account urban ground warming
26
27 71 (Ferguson and Woodbury, 2004). The replacement of natural soil and vegetation by artificial
28
29 72 surfaces increases temperatures of the surrounding air and subsurface throughout the year on
30
31 73 account of indirect solar heating of urban structures, building heat losses and land use change
32
33 74 (Bornstein, 1968). At a district or city level, this phenomenon is called Urban Heat Island effect –
34
35 75 UHI (Landsberg, 1981), and Subsurface Urban Heat Effect – SUHI, when referred to the
36
37 76 thermal effect in the ground (Oke, 1982).

38
39 77 Heat loss from an individual building generates a bulb-shaped volume of subsurface
40
41 78 temperatures that are higher compared to a non-urbanized context (Taniguchi et al., 2007)
42
43 79 Several experimental studies have demonstrated that heat loss from buildings increases the
44
45 80 subsurface temperature by several degrees (generally from 2 to 5 °C) and that this thermal
46
47 81 impact is more persistent in the subsurface rather than in the air. Research on the topic has
48
49 82 been performed in many part of the world, such as Japan (Huang et al., 2009; Taniguchi et al.,
50
51 83 2007), Canada (Ferguson and Woodbury, 2007), Germany (Zhu et al., 2010; Menberg et al.,
52
53 84 2013), Ireland (Allen et al., 2003), Turkey (Yalcin and Yetemen, 2009); United Kingdom
54
55 85 (Headon et al., 2009); Finland (Arola and Korkka-Niemi, 2014) and Switzerland (Rivera et al.,
56
57
58
59
60
61
62
63
64
65

1 86 2017). While calculating and estimating ground temperature distribution is useful in many fields
2 of application, it becomes a key design element of:

3
4 88 - building basements, to minimize heat losses via the ground (e.g. Claesson and
5 Hagentoft, 1991; Hagentoft and Claesson, 1991; Rees et al., 2000),
6 89

7
8 90 - cellars and underground spaces, to ensure appropriate goods storage conditions (e.g.
9 Mazarron et al., 2012; Barbaresi et al., 2014),
10 91

11
12 92 - ground heat exchangers and energy geostructures, to assess shallow geothermal
13 potential and simulate ground thermal behaviour during heat extraction and/or injection (e.g.
14 93 Bandos et al., 2009; Kurevija and Vulin, 2010).
15 94

16
17 95 Dynamic simulators of flow, mass, and heat transfer in the underground are commonly used in
18 the georesources and environmental fields (Pruess and Garcia, 2002; Zhao et al. 2005; Herbert
19 96 and Chillingworth, 2013; Focaccia et al., 2016). In the geothermal sector, it is common practice
20 97 to assign a constant ground temperature value to each subsoil layer as an input parameter. In
21 98 shallow layers, this can be taken as the average ground temperature over the year, which is
22 99 equivalent to the average ambient temperature (Al-Zyoud et al., 2014; Poulsen et al., 2015). In
23 100 other case studies, the shallow layer temperature was experimentally measured in the field over
24 101 a specific time period (Wu et al., 2010; Focaccia, 2013; Barla et al., 2018). In both cases, since
25 102 shallow ground temperature is time dependent, the values assigned did not effectively represent
26 103 the ground temperatures over the whole year. Numerical simulations of underground heat flow
27 104 and mass transfer are not commonly designed to include the thermal effect of aboveground
28 105 structures on ground temperature behaviour in shallow layers. However, identification of
29 106 temperature variations in these shallow layers could improve the efficiency of exploitable
30 107 geothermal energy through the use of energy piles.

31
32
33
34
35
36
37
38
39
40
41
42
43
44
45
46
47
48
49
50
51
52
53
54
55
56
57
58
59
60
61
62
63
64
65

66
67
68
69
70
71
72
73
74
75
76
77
78
79
80
81
82
83
84
85
86
87
88
89
90
91
92
93
94
95
96
97
98
99
100
101
102
103
104
105
106
107
108
109
110
111
112
113
114
115

116
117
118
119
120
121
122
123
124
125
126
127
128
129
130
131
132
133
134
135
136
137
138
139
140
141
142
143
144
145
146
147
148
149
150
151
152
153
154
155
156
157
158
159
160
161
162
163
164
165

166
167
168
169
170
171
172
173
174
175
176
177
178
179
180
181
182
183
184
185
186
187
188
189
190
191
192
193
194
195
196
197
198
199
200
201
202
203
204
205
206
207
208
209
210
211
212
213
214
215
216
217
218
219
220
221
222
223
224
225
226
227
228
229
230
231
232
233
234
235
236
237
238
239
240
241
242
243
244
245
246
247
248
249
250
251
252
253
254
255
256
257
258
259
260
261
262
263
264
265
266
267
268
269
270
271
272
273
274
275
276
277
278
279
280
281
282
283
284
285
286
287
288
289
290
291
292
293
294
295
296
297
298
299
300
301
302
303
304
305
306
307
308
309
310
311
312
313
314
315
316
317
318
319
320
321
322
323
324
325
326
327
328
329
330
331
332
333
334
335
336
337
338
339
340
341
342
343
344
345
346
347
348
349
350
351
352
353
354
355
356
357
358
359
360
361
362
363
364
365
366
367
368
369
370
371
372
373
374
375
376
377
378
379
380
381
382
383
384
385
386
387
388
389
390
391
392
393
394
395
396
397
398
399
400
401
402
403
404
405
406
407
408
409
410
411
412
413
414
415
416
417
418
419
420
421
422
423
424
425
426
427
428
429
430
431
432
433
434
435
436
437
438
439
440
441
442
443
444
445
446
447
448
449
450
451
452
453
454
455
456
457
458
459
460
461
462
463
464
465
466
467
468
469
470
471
472
473
474
475
476
477
478
479
480
481
482
483
484
485
486
487
488
489
490
491
492
493
494
495
496
497
498
499
500
501
502
503
504
505
506
507
508
509
510
511
512
513
514
515
516
517
518
519
520
521
522
523
524
525
526
527
528
529
530
531
532
533
534
535
536
537
538
539
540
541
542
543
544
545
546
547
548
549
550
551
552
553
554
555
556
557
558
559
560
561
562
563
564
565
566
567
568
569
570
571
572
573
574
575
576
577
578
579
580
581
582
583
584
585
586
587
588
589
590
591
592
593
594
595
596
597
598
599
600
601
602
603
604
605
606
607
608
609
610
611
612
613
614
615
616
617
618
619
620
621
622
623
624
625
626
627
628
629
630
631
632
633
634
635
636
637
638
639
640
641
642
643
644
645
646
647
648
649
650
651
652
653
654
655
656
657
658
659
660
661
662
663
664
665
666
667
668
669
670
671
672
673
674
675
676
677
678
679
680
681
682
683
684
685
686
687
688
689
690
691
692
693
694
695
696
697
698
699
700
701
702
703
704
705
706
707
708
709
710
711
712
713
714
715
716
717
718
719
720
721
722
723
724
725
726
727
728
729
730
731
732
733
734
735
736
737
738
739
740
741
742
743
744
745
746
747
748
749
750
751
752
753
754
755
756
757
758
759
760
761
762
763
764
765
766
767
768
769
770
771
772
773
774
775
776
777
778
779
780
781
782
783
784
785
786
787
788
789
790
791
792
793
794
795
796
797
798
799
800
801
802
803
804
805
806
807
808
809
810
811
812
813
814
815
816
817
818
819
820
821
822
823
824
825
826
827
828
829
830
831
832
833
834
835
836
837
838
839
840
841
842
843
844
845
846
847
848
849
850
851
852
853
854
855
856
857
858
859
860
861
862
863
864
865
866
867
868
869
870
871
872
873
874
875
876
877
878
879
880
881
882
883
884
885
886
887
888
889
890
891
892
893
894
895
896
897
898
899
900
901
902
903
904
905
906
907
908
909
910
911
912
913
914
915
916
917
918
919
920
921
922
923
924
925
926
927
928
929
930
931
932
933
934
935
936
937
938
939
940
941
942
943
944
945
946
947
948
949
950
951
952
953
954
955
956
957
958
959
960
961
962
963
964
965
966
967
968
969
970
971
972
973
974
975
976
977
978
979
980
981
982
983
984
985
986
987
988
989
990
991
992
993
994
995
996
997
998
999
1000

1 116 temperature and humidity measurement campaign. Measurements had been taken inside the
 2 117 building (Barbaresi et al., 2014), in the surrounding undisturbed ground at different depths (Tinti
 3 118 et al., 2014), inside the building cellar (Barbaresi et al., 2015) and beside and below the building
 4 119 at different depths (Tinti et al., 2015). Calculations and modeling were performed to improve
 5 120 cellar air temperature management (Benni et al., 2016) and estimate ground temperature
 6 121 evolution as a result of the building's presence (Tinti et al., 2017a).

12 122 **2. Materials and methods**

13 123 *2.1. Choice of the numerical simulator*

14 124 The numerical simulator *FEFLOW*[®] (Finite Element Flow simulator), commonly used in the
 15 125 shallow geothermal sector (Al-Khoury et al., 2005; Al-Khoury et al., 2006), was chosen for
 16 126 setting optimization. *FEFLOW*[®] is an integrated package including dynamic flow, heat and mass
 17 127 transportation simulation tools. It allows users to create as many layers as necessary and
 18 128 upload node by node database information for each layer (hydraulic properties, thermal
 19 129 properties, initial conditions of temperature and water level).

20 130 *2.2. Model parameters: geology, hydrogeology and building dimensions.*

21 131 The case study involved a two-storey building with an underground wine-ageing room in a rural
 22 132 area in the countryside of Bologna (Italy). The bearing is 32° north-east. The building's key
 23 133 features are reported in *Table 1*.

24 134 *Table 1: Key building features.*

	Two-storey building	Wine-ageing room
Width	9.8 m	5.6 m
Length	20.5 m (above ground) + 5.6 m (above cellar)	9.8 m
Height	7.3 m (borders), 8.4 m (centre)	2.6 m (underground)
Walls	25.0 cm thick masonry	25.0 cm thick masonry
Floor	30.0 cm hollow concrete slab	20.0 cm concrete slab
Ceiling	-	30.0 cm hollow concrete slab
Air conditioning	Heating and natural ventilation	Natural ventilation

25 135 A model PCE-FWS20 weather station located 100 m from the building collected the main
 26 136 weather data. The two-storey building is heated during the winter season, and there is no
 27 137 mechanical cooling during summer. A set of stand-alone temperature and humidity data
 28 138 loggers, model PCE-HT71, with a 0.1°C resolution, an accuracy of ±0.5°C and a 1 minute
 29 139 registration interval were chosen to collect data. Three were used to measure the internal

1
2
3
4
5
6
7
8
9
10
11
12
13
14
15
16
17
18
19
20
21
22
23
24
25
26
27
28
29
30
31
32
33
34
35
36
37
38
39
40
41
42
43
44
45
46
47
48
49
50
51
52
53
54
55
56
57
58
59
60
61
62
63
64
65

140 ambient data (temperature and humidity) of the rooms of the two-storey building (Barbaresi et
141 al., 2014). Seventeen data loggers were subsequently placed inside the exclusively naturally
142 ventilated wine cellar (Barbaresi et al., 2015).
143 Subsoil temperature distribution in the intervention area had already been thoroughly analysed.
144 Four monitoring boreholes, each with three data loggers, with integrated temperature sensors,
145 placed at different depths, were drilled at designated positions with respect to the building.
146 Boreholes I and II are vertical and are both equipped with three data loggers at depths of 2, 4
147 and 6 m (Numbered 1 to 6, Tinti et al., 2014). Borehole III, with a total length of 17 m, is inclined
148 (10° from horizontal plane) and has 3 data loggers at depths of 1.8, 2.6 and 3.7 m, 2 of them
149 (the deepest ones) being located below the building and beside the cellar (Numbered 7, 8 and
150 9, Tinti et al., 2015). Borehole IV is vertical and shallower than the others. It has 3 data loggers
151 at depths of 0.10, 0.65 and 1.20 m (Numbered 10, 11 and 12, Tinti et al., 2015). The whole
152 intervention area and the location of the 3 measurement points on Borehole III with respect to
153 the underground cellar, are shown in *Figure 1*.

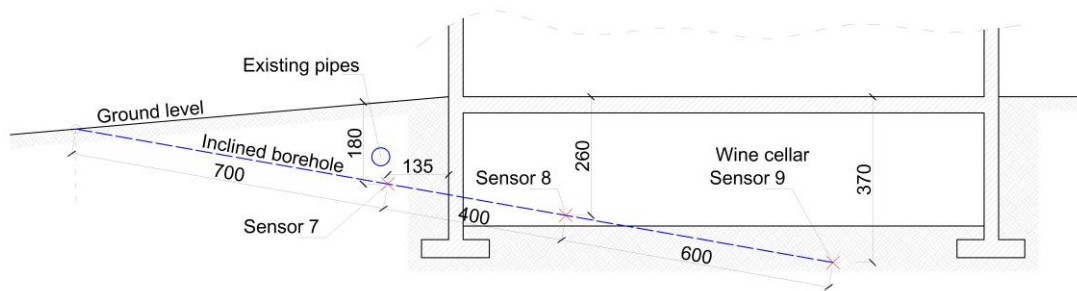
154

1
2
3
4
5
6
7
8
9
10
11
12
13
14
15
16
17
18
19
20
21
22
23
24
25
26
27
28
29
30
31
32
33
34
35
36
37
38
39
40
41
42
43
44
45
46
47
48
49
50
51
52
53
54
55
56
57
58
59
60
61
62
63
64
65



155

Section A-A



156

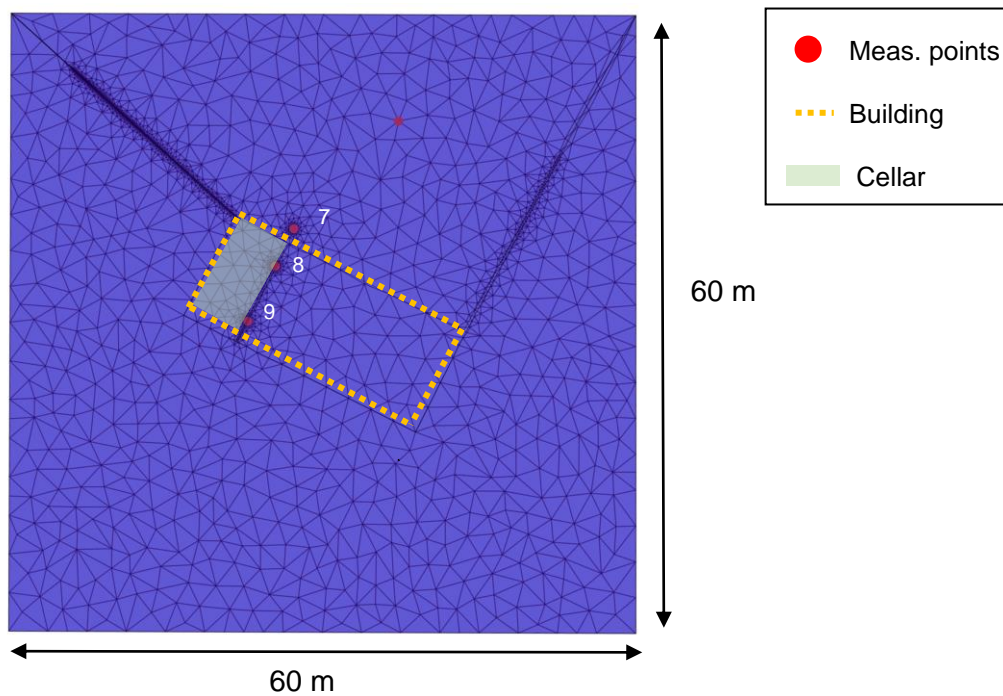
157

158 *Figure 1. Intervention area (up) and vertical section of the underground cellar, with localization*
 159 *of the three measurement points (down).*

160

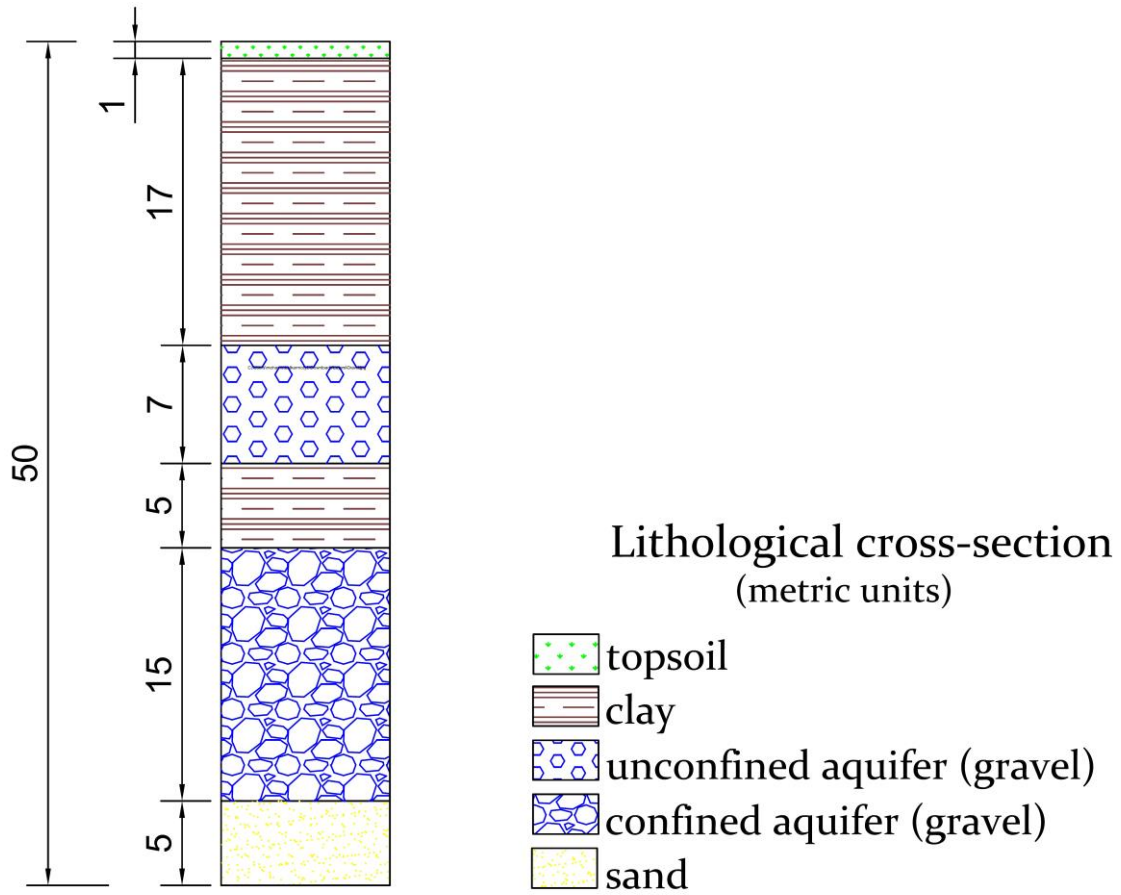
161 The shallow underground of the whole area is prevalently composed of low moist clay down to a
162 depth of 6 m, even lower in some places. Data sources are the geological investigations related
163 to the installation of data loggers. All geological data were collected by the borehole data
164 loggers.

165 The model domain implemented in *FEFLOW*[®] extends beyond the building itself for a total
166 surface area of 60x60 m, a depth of 50 meters and 0.25 meters of boundary surface area, the
167 latter chosen to guarantee a swathe of undisturbed ground around the boundary of the house. A
168 tetrahedral mesh was used with refinement regions close to three observation points,
169 corresponding to measurement points 7, 8 and 9. The finite elements generated range from
170 $5 \cdot 10^{-2} \text{ m}^2$ in the zones close to the sensors to 5 m^2 from the building (*Figure 2*).



171 *Figure 2. Mesh of the area chosen for the dynamic simulation.*

172 A series of 18 layers was used to detail the geology of the area as well as a first buffer layer.
173 Geological detail up to 50 m was obtained from the Geological Survey of the Emilia Romagna
174 Region (*Figure 3*). The study does not consider groundwater flow in the two aquifers located
175 respectively at 18 m and 30 m below the ground surface since their thermal impact is nil with
176 respect to the intervention area (between 0.5 and 10 m below the ground surface).



177

178 *Figure 3: Lithological cross-section for the case study (from Tinti et al., 2017a).*

179 Measurement points 7, 8 and 9, expressed in relation to the cellar and building walls, are given
 180 in *Table 2*. All of them are located in low moist clay.

181 *Table 2. Localization of measurement points 7, 8 and 9.*

Sensor number	Depth (m)	Qualitative localization	Orthogonal distance from the building northern wall (m)	Geological layer number (refer to <i>Table 4</i>)
7	1.8	Beside the building and cellar walls	+1.35	6
8	2.6	Under the building, beside the cellar wall	-2.57	7
9	3.7	Under the building, under the cellar	-8.47	9

182 **2.3. Model boundaries: ground and building temperature**

183 The basic equation for assessing vertical temperature (T_g) distribution at low depth is a function
 184 of the ambient temperature wave and the thermal properties of the ground (Kusuda and
 185 Achenbach, 1965). Since all the function variables are regionalized, the target variable is four

186 dimensional, varying in space (x,y,z) and time (t) . Since T_g has a sinusoidal behaviour, the year
 187 is usually given as a wave period.

188 *Equation 1* summarizes the well-known distribution of temperatures in the subsoil at low depths
 189 (Baggs, 1985).

190
$$T_g(x,y,z,t) = T_{me}(x,y) - A_e(x,y) \cdot \exp\left[-z \cdot \sqrt{\left(\frac{\pi}{365 \cdot \alpha(x,y,z)}\right)}\right] \cdot \cos\left[\frac{2 \cdot \pi}{365} \cdot \left(t - t_{T_0}(x,y) - \frac{z}{2} \cdot \sqrt{\frac{365}{\pi \cdot \alpha(x,y,z)}}\right)\right]$$

191 1.

192 Where:

193 T_g is the space-time varying underground temperature (°C),

194 T_{me} is the annual surface average temperature (°C),

195 A_e is the annual surface wave amplitude (°C),

196 t_{T_0} is the time at minimum temperature (days),

197 α is the equivalent thermal diffusivity (m²/days).

198 Although other parameters such as the vegetation coefficient, the insulation coefficients, and the
 199 geothermal heat flow, can be included in the analytical equation, we decided to omit these in the
 200 present work since our aim was to define settings to recreate the bulb-shaped volume of
 201 subsurface temperatures below a building in the numerical simulator without the inclusion of
 202 corrective coefficients. In addition, since the area of investigated was limited to the shallow
 203 layers, disregarding the contribution of geothermal heat flow was in this case an acceptable
 204 simplification.

205 Experimental temperature measurement in Boreholes I and II (Tinti et al., 2014) allowed
 206 estimation of ground thermal wave parameters by non-linear regression based on *Equation 1*.
 207 Parameters obtained by non-linear regression are summarized in *Table 3*.

208 *Table 3. Entering parameters to estimate ground temperature in the survey area with the*
 209 *analytical method.*

Yearly ambient temperature (°C)	Yearly amplitude (°C)	Day of minimum temperature (days)	Ground thermal diffusivity (m ² /days)
15.0	15.5	10 th	0.0288

210 January 10th is statistically the day of minimum temperature in the climatic area of Bologna, so
 211 in the climatic wave it represents the position of the inflection point.

213 Since the ground was considered homogeneous in the survey area, no spatial variations were
 214 attributed to parameters. The temperature of the ground below the study area (i.e. from 18 m)
 215 was calculated also considering geological and hydrogeological variations, as reported in Tinti
 216 et al., 2017a. Since the effect of deep temperature on the surface layers is very limited, no
 217 further investigations were conducted during this study below 18 m. The temperatures indicated
 218 by Tinti et al., 2017a were used in the dynamic simulator as boundary and initial conditions. The
 219 baseline condition for each layer was that layer's average temperature on 1st January (starting
 220 date of the simulation) as shown in *Table 4*, while the Dirichletian boundary conditions at the
 221 borders of each layer were represented as the time-varying temperature evolution over the year.
 222 As no groundwater flow was considered, a Dirichletian boundary condition of 0 m hydraulic
 223 head was set for all the sides and layers of the model.

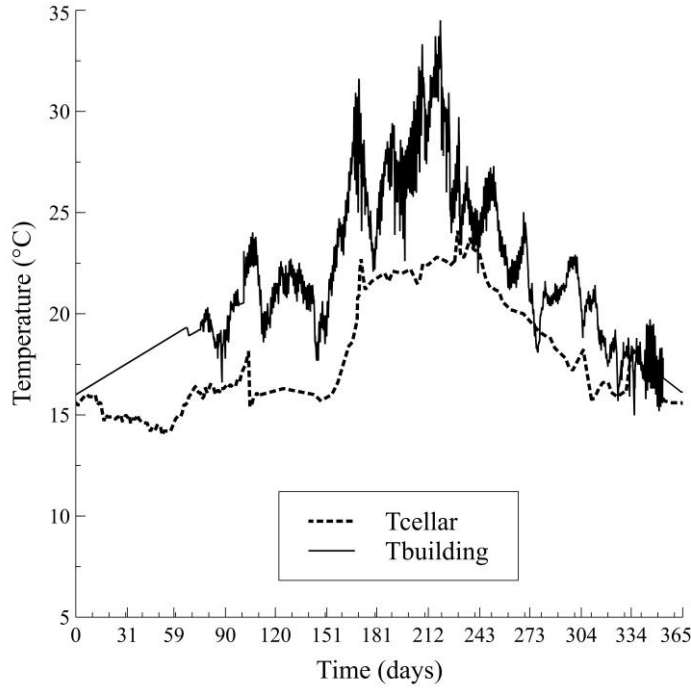
224 *Table 4. Initial temperature conditions for each layer of the model.*

Layer n°	Thickness (m)	Depth (m)	Initial temperature (°C)
2	0.25	0.25	4.67
3	0.25	0.50	6.24
4	0.50	1.00	7.80
5	0.50	1.50	10.44
6	0.50	2.00	12.51
7	0.50	2.50	13.47
8	0.50	3.00	14.96
9	1.00	4.00	15.85
10	2.00	6.00	16.45
11	2.00	8.00	16.10
12	2.00	10.00	15.58
13	2.00	12.00	15.52
14	6.00	18.00	15.66
15	7.00	25.00	15.93
16	5.00	30.00	15.37
17	15.00	45.00	15.84
18	5.00	50.00	15.60

225 The ground profile was defined based on the lithological section (*Figure 3*). Layers 2 to 4 are all
 226 part of the first lithological type (topsoil); layers 5 to 14 are part of the second lithological type
 227 (clay). Both were refined to obtain better representation of the superficial layers, which are
 228 mostly influenced by the external temperature. In contrast, layers 15 to 18 were defined
 229 according to the original thickness of each lithological type.

230 The basement of the two-storey building was considered as corresponding to the top of Layer 2.
 231 Since Layer 1 was considered an ambient temperature buffer, Layer 2 was considered as
 232 located at 0 m depth. The time-varying temperature over the year registered inside the building
 233 ($T_{building}$) at this 0 m depth was considered as the Dirichletian boundary. The basement of the

234 wine ageing room was, on the other hand, placed at the top of Layer 8 (located at a depth of 3
 235 m). The Dirichletian boundary condition at this depth was the time-varying temperature over the
 236 year registered in the wine room (T_{cellar}). Figure 4 shows the reference temperatures inside the
 237 building and cellar over one year during the study.



238

239 *Figure 4. Internal temperature of building and cellar*

240 The two temperature evolutions were used as wall temperature conditions in the simulation to
 241 express the heat effect of the building.

242 *2.4. Model parameters: thermal conductivity, heat capacity and effective porosity*

243 Each of the 18 layers was characterized in terms of thermal properties, namely thermal
 244 conductivity, thermal capacity, and effective porosity. Respective values are shown in Table 5.

245 For the specific case study, the value of thermal diffusivity was calculated through the multiyear
 246 measurement campaign up to a depth of 6 m. The value was later additionally verified by a
 247 Thermal Response Test (TRT) performed on a geothermal basket installed on site (Ferrari et
 248 al., 2016; Tinti et al., 2017b).

249 Other parameters were obtained on the basis of the relationship between thermal diffusivity and
 250 conductivity, as shown in Equation 2.

251

$$\alpha = \frac{\lambda}{\rho \cdot C}$$

252 2.

253 Where

254 λ is the equivalent thermal conductivity (W/(m·K)),

255 ρ is the density (kg/m³),

256 C is the heat capacity (J/(kg·K)),

257 $\rho \cdot C$ is the volumetric heat capacity (J/(m³·K)).

258 Lithology-based bibliographic values were taken for the layers deeper than 18 m below the
259 ground surface (Tinti et al., 2017a). Effective porosity was set at 10% (i.e. low effective porosity,
260 typical of low moist clay) down to the first aquifer (18 m deep), where it was increased up to
261 30%. Effective porosity was used in the simulation to estimate the amount of water in the aquifer
262 and the quantity of air in the dry layers. This, together with the thermal conductivity and
263 volumetric heat capacity provided for each of the lithologies generated the actual thermal
264 properties of each layer.

265 *Table 5. Thermal characteristics associated with the layers.*

Layer n°	Thickness (m)	Depth (m)	Thermal conductivity (W/(m·K))	Volumetric heat capacity (MJ/(m ³ ·K))	Effective porosity (-)
2	0.25	0.25	0.50	1.0	0.1
3	0.25	0.50	0.65	1.5	0.1
4	0.50	1.00	0.65	1.5	0.1
5	0.50	1.50	0.65	1.5	0.1
6	0.50	2.00	0.65	1.5	0.1
7	0.50	2.50	0.65	1.5	0.1
8	0.50	3.00	0.65	1.5	0.1
9	1.00	4.00	0.65	1.5	0.1
10	2.00	6.00	0.65	1.5	0.1
11	2.00	8.00	0.65	1.5	0.1
12	2.00	10.00	0.65	1.5	0.1
13	2.00	12.00	0.65	1.5	0.1
14	6.00	18.00	0.65	1.5	0.1
15	7.00	25.00	1.80	2.4	0.3
16	5.00	30.00	1.00	1.6	0.3
17	15.00	45.00	1.80	2.4	0.3
18	5.00	50.00	2.40	2.4	0.3

266 A thermal conductivity of 0.35 W / (m·K) was assigned to the building walls and floors. This
267 represents the characteristic thermal conductivity of a hollow concrete slab with a high degree of
268 insulation.

269 3. Results

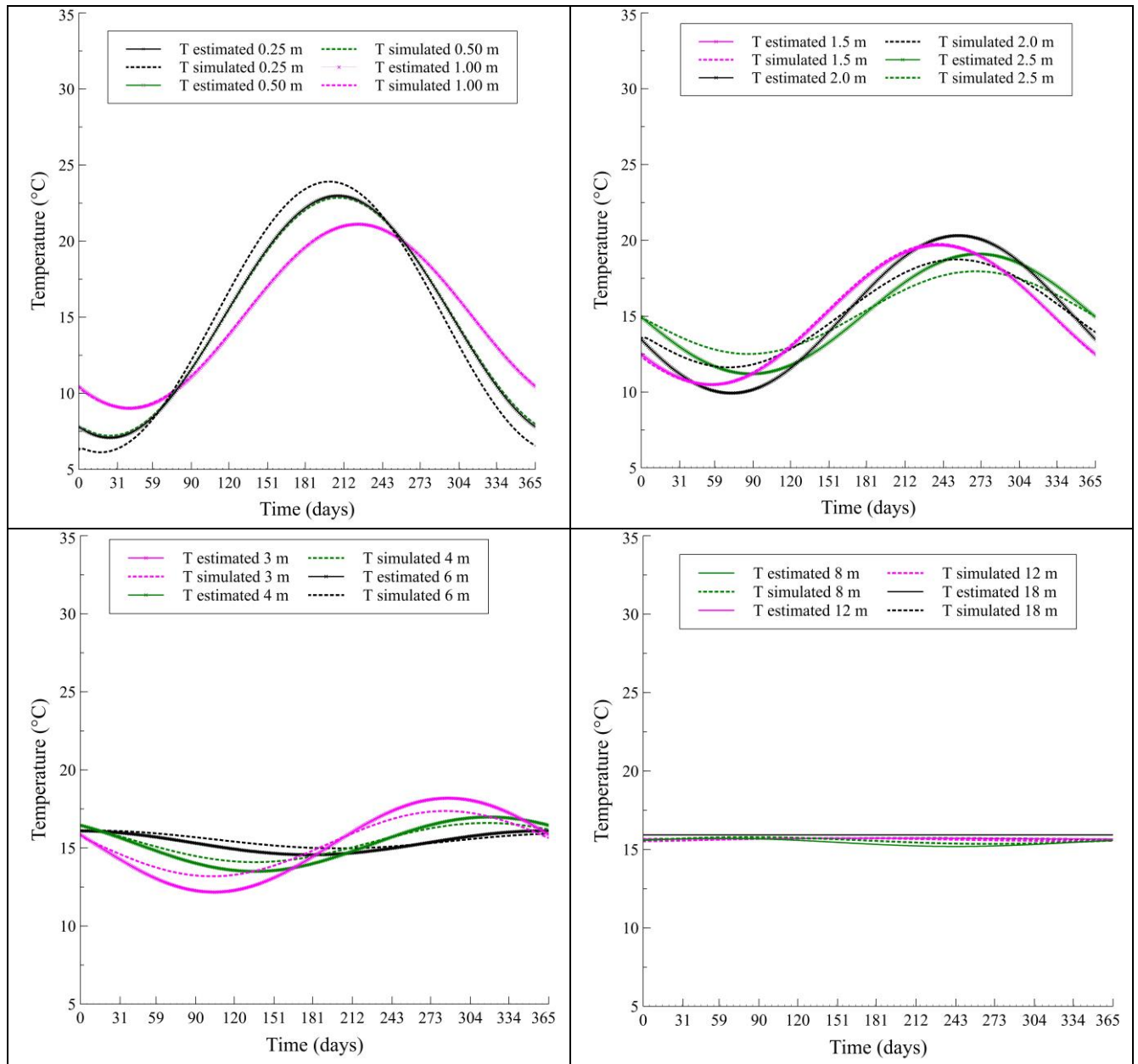
1 270 The above model, implemented in *FEFLOW*[®], was run for 1825 days under the boundary and
2 271 initial conditions described. The initial time step was set at 0.5 days and subsequently defined
3
4 272 automatically by the convergence of the equations. Local temperatures at the measurements
5
6 273 points were retrieved from the simulation each day and compared with the on-site
7
8 274 measurements and estimated data based on non-linear regression on *Equation 1*. The
9
10 275 undisturbed ground temperature of each layer was recorded along a vertical profile at
11
12 276 observation points positioned one on top of the other at 15 m from the building (where the heat
13
14 277 island effect is negligible). Since the new dynamic boundary conditions settle after 2 years of
15
16 278 simulation, comparison between simulated and estimated natural ground temperatures can be
17
18 279 made taking either the 3rd, 4th or 5th year of simulation (*Equation 1*). In this study we carried out
19
20 280 the comparison on the basis of simulated temperatures of the 5th year.

21
22 281 The match between simulated and estimated values of space-time varying ground temperature
23
24 282 was obtained in all parts of the domain (including below the building and beside the cellar) using
25
26 283 the following settings:

- 27
28 284 • Tetrahedral mesh refined around sensor positions, where observation points were defined;
- 29
30 285 • Initial temperatures of the different layers set equal to the average 1st January temperature;
- 31
32 286 • Dirichletian boundary conditions for the temperature of each layer equal to the time-varying
33
34 287 evolution of each layer temperature over the year;
- 35
36 288 • Dirichletian boundary condition for building wall temperature equal to the time-varying
37
38 289 temperature registered over the year inside the building;
- 39
40 290 • Dirichletian boundary condition for cellar wall temperature equal to the time-varying
41
42 291 temperature registered over the year inside the cellar;
- 43
44 292 • Dirichletian boundary condition of 0 m hydraulic head set throughout the model.

45 46 47 293 3.1. *Reconstruction of undisturbed underground temperature*

48
49 294 The comparison between simulated and estimated values of ground temperature evolution is
50
51 295 presented in *Figure 5*. Ground temperatures at the different depths were estimated using non-
52
53 296 linear regression based on *Equation 1*, and validated at the different depths (2, 4 and 6 m)
54
55 297 against those measured (Tinti et al., 2014).



298 *Figure 5. Comparison between simulated and estimated temperatures at different depths.*

299

300 *Table 6* reports the average simulated wave error with respect to that estimated at each depth.

301 The values estimated with non-linear regression are considered as reference values. Error

302 tends to decrease with depth because the temperature becomes more homogeneous.

303

304 *Table 6. Maximum, minimum and average error of the simulated ground temperature at different*

305 *depths compared to the estimated values by non-linear regression of Equation 1 on*

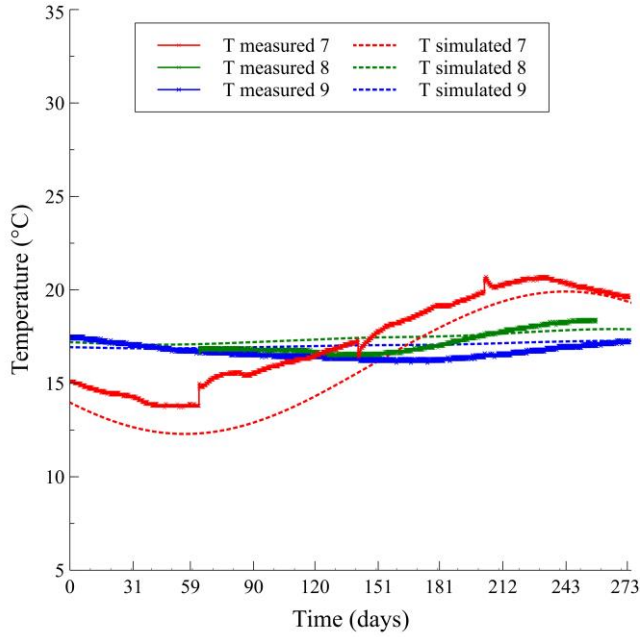
306 *measurement points (Tinti et al., 2014).*

Depth (m)	Maximum Relative Error (%)	Minimum Relative Error (%)	Average Relative Error (%)
0.00	6.1%	0.0%	2.2%
0.25	5.5%	0.0%	2.1%
0.50	5.1%	0.0%	2.3%
1.00	4.7%	0.0%	2.3%
1.50	17.8%	0.1%	9.3%
2.00	13.4%	0.0%	7.3%
2.50	10.3%	0.0%	5.8%
3.00	6.3%	0.0%	3.6%
4.00	4.4%	0.0%	2.5%
6.00	1.9%	0.0%	0.9%
8.00	0.7%	0.0%	0.3%
10.00	0.4%	0.0%	0.2%
12.00	1.5%	1.4%	1.5%
18.00	2.1%	1.9%	2.0%

308 **3.2. Reconstruction of sensor recorded temperatures.**

309 The temperatures measured at points 7, 8 and 9 were compared with the products of the
 310 simulation. Since the three investigation points come within the impact area affected by building
 311 heat loss, the values returned at these points do not follow the natural ground thermal state.

312 *Figure 6* shows the comparison.



313

314 *Figure 6. Comparison between simulated and measured temperature values beside and below*
 315 *the building at measurement points 7 (1.8 m), 8 (2.6 m) and 9 (3.7 m).*

316 The comparison led to the average error presented in *Table 7*.

317 *Table 7. Maximum, minimum and average error of the simulated sensor-based temperature*
 318 *compared to the actual values measured.*

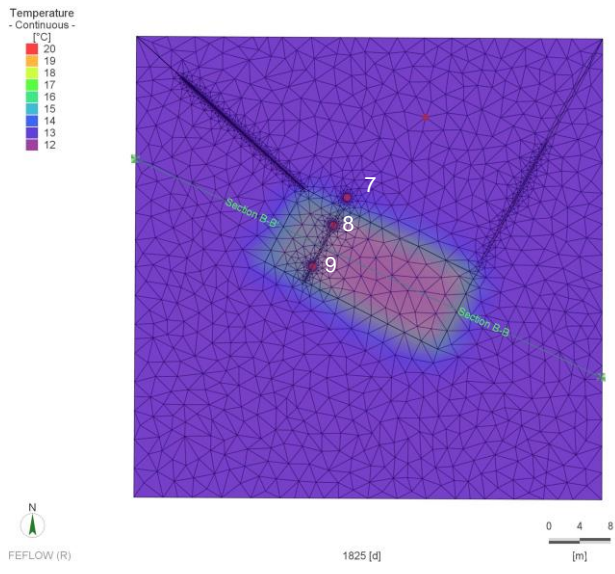
Sensor	Depth	Maximum Relative Error	Minimum Relative Error	Average Relative Error
7	1.8 m	19.4%	0.8%	9.0%
8	2.6 m	6.1%	0.1%	2.4%
9	3.7 m	5.3%	0.1%	2.8%

319 The low average error shows that the settings were correctly chosen to include the building's
 320 thermal contribution in the dynamic simulator.

321 *3.3. Simulation of building thermal effect on the ground*

322 Having calibrated the model by comparing simulated and measured data, it was then possible to
 323 simulate the entire ground thermal behaviour as affected by the building over time. The results
 324 for four characteristic periods of January, April, July and October are given in section *B-B* of
 325 *Figure 7*. Ground temperature evolution is shown in *Figure 8*.

1
2
3
4
5
6
7
8
9
10
11
12
13
14
15
16
17
18
19
20
21
22
23
24
25
26
27
28
29
30
31
32
33
34
35
36
37
38
39
40
41
42
43
44
45
46
47
48
49
50
51
52
53
54
55
56
57
58
59
60
61
62
63
64
65

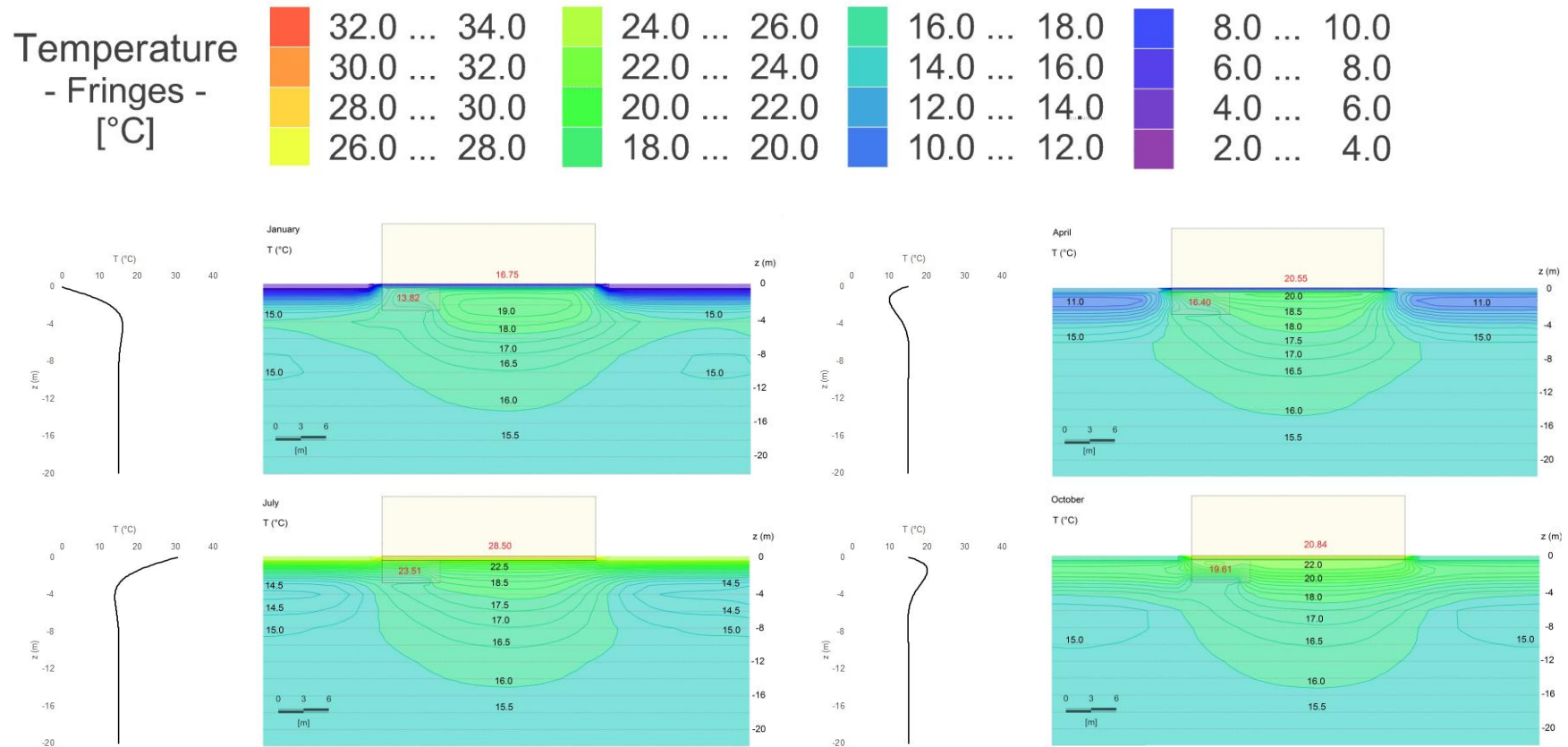


326

327 *Figure 7 Simulated area and definition of Section B-B.*

328
329
330
331
332
333
334
335
336
337
338
339
340
341
342
343
344
345
346
347
348
349
350
351
352
353
354
355
356
357
358
359
360
361

16
17
18
19
20
21
22
23
24
25
26
27
28
29
30
31
32
33
34
35
36
37
38
39
40
41
42
43
44
45
46
47
48
49
50
51
52
53
54
55
56
57
58
59
60
61
62
63
64
65



362

363 *Figure 8. Section B-B showing ground thermal behaviour affected by the presence of the building and cellar in the characteristic months of January, April,*
 364 *August and October. For each month, the following items are shown: temperature isolines in the ground (black numbers), average temperature in the*
 365 *above ground building and the cellar (red numbers), temperature profile used as boundary condition (black line).*

1 366 Simulation of ground temperature evolution under the building follows the bulb-shaped pattern
2 367 described consistently in the literature and presented in the introduction to this paper.
3
4 368 Temperature variation with depth is notably vertically dampened compared with the undisturbed
5
6 369 ground, with no relevant changes occurring over time. This is because the building acts as an
7
8 370 insulator against the external weather. Below the building, at depths from 2 to 8 m, temperature
9
10 371 remains constant throughout the year at around 17-18°C. In contrast, temperatures around the
11
12 372 building down to 4 m depth, in winter, vary from 2 to 15 °C, while, in summer, vary from 28 to
13
14 373 14.5°C. From 4 down to 8 m, there is a transitional zone, with very low temperature variations
15
16 374 along the year, while below 8 m temperature remains constant in time.
17
18 375 The numerical simulation also evidences the thermal contribution of the indoor air temperature
19
20 376 of the cellar, which slightly affects the temperatures of its surroundings.
21
22 377 Being validated by the measurements taken, the simulation values may be used in the design of
23
24 378 energy geostructures and ground heat exchangers when these are located below buildings.
25
26 379 Results can be used both directly in *FEFLOW*[®] as initial conditions for further simulations of
27
28 380 geothermal energy exploitation or extrapolated for the dedicated design of energy geostructures
29
30 381 and ground heat exchanger fields.
31
32 382 Since the heat exchange rates of ground heat exchangers in winter and summer are
33
34 383 proportional to initial ground temperature, it follows that exchanger systems for standard heating
35
36 384 and cooling loads will be more profitable below a building than underneath an uncovered area.
37
38 385 So correct simulation in all grid nodes improves the quality of design. Considering the correct
39
40 386 thermal impact of buildings on the ground should lead to more precise forecasts of geothermal
41
42 387 energy exploitation rates for heating and cooling needs.
43
44

45 **388 4. Conclusions**

46
47 389 The study defined optimal settings to reconstruct the time-space varying temperature field
48
49 390 deriving from the presence of a building in a dynamic simulator. The settings were calibrated
50
51 391 performing numerical simulation and comparing the results with ground temperature values
52
53 392 measured on site in a rural area beside and below a detached building. As far as the authors
54
55 393 are aware, this is one of the few studies of its kind. It could pave the way for better thermal
56
57 394 behaviour simulation, which would lead to improved energy geostructures and ground heat
58
59
60
61
62
63
64
65

1 395 exchanger design. In particular, the results of this paper are especially pertinent for ground heat
2 396 exchanger design in urban areas, where the presence of buildings can considerably affect
3
4 397 thermal system performance. This is especially the case of energy piles with absorption pipes
5
6 398 installed below buildings, where standard climate-dependent ground thermal conditions do not
7
8 399 apply. Moreover, energy pile length is usually limited to a few meters below any building, with
9
10 400 the result that thermal losses from buildings will have a large impact on energy performance.
11
12 401 The study further underlines that the exploitable energy used by shallow ground heat
13
14 402 exchangers located in urban areas is only in part 'natural' (renewable geothermal and solar
15
16 403 energy) since heat recovery of energy losses from buildings and districts (subsurface urban
17
18 404 heat island effect) make up a sizeable component of the energy available to these systems.
19
20 405 Further studies will be performed to quantify this contribution in the short and long term, both for
21
22 406 energy geostructures located below single buildings and for ground heat exchanger fields
23
24 407 located in an urban area, with estimation and simulation of the effect of multiple buildings on
25
26 408 ground heat exchanger fields.

28 29 409 **Acknowledgements**

30
31 410 The Authors wish to thank the Branchini 1858 winery of Toscanella di Dozza (BO), Italy for their
32
33 411 collaboration during of the monitoring and experimental trials. Thanks also go to all the co-
34
35 412 workers and technicians of University of Bologna who over the years have helped install,
36
37 413 improve and maintain the monitoring system.

38 39 40 414 **References**

41
42 415 Al-Khoury R, Bonnier PG and Brinkgreve R.B.J. (2005) Efficient finite element formulation for
43
44 416 geothermal heating systems. Part I: steady state. International Journal for Numerical Methods in
45
46 417 Engineering **63(7)**: 988 - 1013
47
48 418 Al-Khoury R and Bonnier PG (2006) Efficient finite element formulation for geothermal heating
49
50 419 systems. Part II: transient. International Journal for Numerical Methods in Engineering.
51
52 420 **67(5)**:725 - 745.
53
54 421 Al-Zyoud S., Rühaak W. and Sass I. (2014) Dynamic numerical modelling of the usage of
55
56 422 groundwater for cooling in north east Jordan. A geothermal case study. Renewable Energy **62**:
57
58 423 63 - 72
59
60
61
62
63
64
65

- 1 424 Allen A., Milenic D. and Sikora P. (2003) Shallow gravel aquifers and the urban 'heat island'
2 425 effect: a source of low enthalpy geothermal energy. *Geothermics* **32(4)**: 569 – 578.
3
4 426 Arola T. and Korkka-Niemi K. (2014) The effect of urban heat islands on geothermal potential:
5 427 examples from Quaternary aquifers in Finland. *Hydrogeology Journal* **22(8)**: 1953 – 1967,
6 428 <https://doi.org/10.1007/s10040-014-1174-5>.
7
8 429 Baggs S.A. (1985) Remote prediction of ground temperature in Australian soils and mapping its
9 430 distribution. *Solar Energy* **30(4)**: 351 –366.
10
11 431 Bandos T.V., Montero A., Fernandez E., Santander J.L.G., Isidro J.M. et al. (2009) Finite line-
12 432 source model for borehole heat exchangers: effect of vertical temperature variations.
13 433 *Geothermics* **38(2)**: 263 - 270.
14
15 434 Barbaresi A., Torreggiani D., Benni S. and Tassinari P. (2014) Underground cellar thermal
16 435 simulation: definition of a method for modelling performance assessment based on experimental
17 436 calibration. *Energy and Buildings* **76**: 363–372.
18
19 437 Barbaresi A., Torreggiani D., Benni S. and Tassinari P. (2015) Indoor air temperature
20 438 monitoring: A method lending support to management and design tested on a wine-aging room.
21 439 *Building and Environment* **86**: 203 – 210.
22
23 440 Barla M., Di Donna A. and Baralis M. (2018) City-scale analysis of subsoil thermal conditions
24 441 due to geothermal exploitation. *Environmental Geotechnics*, ahead of print.
25 442 <https://doi.org/10.1680/jenge.17.00087>.
26
27 443 Benni S., Tinti F., Barbaresi A., Ferrari M., Bruno R. et al. (2016) Experimental models of
28 444 underground temperature for decision making in wine cellar design. In *Proceedings of 44th*
29 445 *International Symposium on Agricultural Engineering*. (Kovačev I. and Zrnčić H. (eds)).
30 446 Sveučilište u Zagrebu, Agronomski fakultet, Zavod za mehanizaciju poljoprivrede, Zagreb, HR,
31 447 pp. 487 - 498.
32
33 448 Bornstein R.D. (1968) Observation of the Urban Heat Island effect in New York City. *Journal of*
34 449 *Applied Meteorology* **7(4)**: 575 - 581.
35
36 450 Cermak, V., and Rybach, L. (1979) *Terrestrial heat flow in Europe*. Springer Verlag, ISBN
37 451 10:3540094407/ISBN 13:978354009440.
38
39 452 Claesson J. and Hagentoft C-E. (1991) Heat loss to the ground from a building – I. General
40 453 theory. *Building and Environment* **26(2)**: 95-208.
41
42
43
44
45
46
47
48
49
50
51
52
53
54
55
56
57
58
59
60
61
62
63
64
65

1 454 Ferguson G. and Woodbury A.D. (2004) Subsurface heat flow in an urban environment. Journal
2 455 of Geophysical Research **109(B2)**: B02402.
3
4 456 Ferguson G. and Woodbury A. D. (2007) Urban heat island in the subsurface. Geophysical
5
6 457 Research Letters, **34(23)**: L23713.
7
8 458 Ferrari M., Barbaresi A., Tinti F., Brunelli D., Benni S., Verdecchia A. Bedeschi E., Bruno R.,
9
10 459 Tassinari P. (2016) Performance evaluation of a homemade cylindrical basket heat exchanger,
11
12 460 by a multi-sensors monitoring campaign. In *Proceedings of European Geothermal Energy*
13
14 461 *Conference 2016*. EGEC, Brussels, B. pp. 1-10.
15
16 462 Focaccia S. (2013) Thermal response test numerical modeling using a dynamic simulator.
17
18 463 Geothermal Energy **1(3)**: pp. 12
19
20 464 Focaccia S., Tinti F., Monti F., Amidei S. and Bruno R. (2016) Shallow geothermal energy for
21
22 465 industrial applications: A case study. Sustainable Energy Technologies and Assessments **16**: 93
23
24 466 - 105,
25
26 467 Hagentoft C-E and Claesson J. (1991) Heat loss to the ground from a building – II. Slab on the
27
28 468 ground. Building and Environment **26(4)**: 395 - 403.
29
30 469 Headon J., Banks D., Waters A. and Robinson V. K. (2009) Regional distribution of ground
31
32 470 temperature in the Chalk aquifer of London, UK. Quarterly Journal of Engineering Geology &
33
34 471 Hydrogeology **42(3)**: 313 - 323.
35
36 472 Herbert A. S. and Chillingworth G. (2013) Thermal modelling of large scale exploitation of
37
38 473 ground source energy in urban aquifers as a resource management tool. Applied Energy **109**:
39
40 474 94–103.
41
42 475 Huang S., Taniguchi M., Yamano M. and Wang C. H. (2009) Detecting urbanization effects on
43
44 476 surface and subsurface thermal environment-a case study of Osaka. Science of the Total
45
46 477 Environment **407(9)**: 3142 - 3152
47
48 478 Kurevija T. and Vulin D. (2010) Determining undisturbed ground temperature as part of shallow
49
50 479 geothermal resources assessment. Rudarsko-Geolosko-Naftni Zbornik **22**: 27-36.
51
52 480 Kusuda T. and Achenbach P. (1965) Earth temperature and thermal diffusivity at selected
53
54 481 stations in the United States, ASHRAE Transactions **71**: 61 - 75.
55
56 482 Landsberg, H. E. (1981) The Urban Climate. International Geophysics Series **28**: 275.
57
58
59
60
61
62
63
64
65

1 483 Mazarron F.R., Cid-Falceto J. and Canas I. (2012) Ground thermal inertia for energy efficient
2 484 building design: a case study on food industry. *Energies* **5(2)**: 227 - 242.
3
4 485 Menberg K., Bayer P., Zosseder K., Rumohr S. and Blum P. (2013): Subsurface urban heat
5 486 islands in German cities. *Science of Total Environment* **442**: 123–133.
6
7 487 Oke, T. R. (1982) The energetic basis of the urban heat island *Quarterly Journal of the Royal*
8 488 *Meteorological Society* **108(455)**: 1 – 24
9
10 489 Pouloupatis P.D., Florides G., Tassou S. (2011) Measurements of ground temperatures in
11 490 Cyprus for ground thermal applications. *Renewable Energy* **36(2)**: 804–814.
12
13 491 Poulsen S.E., Balling N. and Nielsen S.B. (2015) A parametric study of the thermal recharge of
14 492 low enthalpy geothermal reservoirs. *Geothermics* **53**: 464-478.
15
16 493 Pruess K. and Garcia J., (2002) Multiphase flow dynamics during CO₂ disposal into saline
17 494 aquifers. *Environmental Geology* **42(2-3)**: 282 - 295.
18
19 495 Rees S.W., Adjali M.H., Zhou Z., Davies M. and Thomas H.R. (2000) Ground heat transfer
20 496 effects on the thermal performances of earth-contact structures. *Renewable and Sustainable*
21 497 *Energy Reviews* **4(3)**: 213 - 265.
22
23 498 Rivera J.A., Blumm P. and Bayer P. (2017) Increased ground temperatures in urban areas:
24 499 Estimation of the technical geothermal potential. *Renewable Energy* **103**: 388 – 400.
25
26 500 Taniguchi M, Uemura T. and Jago-on K. (2007) Combined effects of urbanization and global
27 501 warming on subsurface temperature in four Asian cities. *Vadose Zone Journal* **6**: 591–596.
28
29 502 Tinti F., Barbaresi A., Benni S., Torreggiani D., Bruno R. et al. (2014) Experimental analysis of
30 503 shallow underground temperature for the assessment of energy efficiency potential of
31 504 underground wine cellars. *Energy and Buildings* **80**: 451 - 460.
32
33 505 Tinti F., Barbaresi A., Benni S., Torreggiani D. Bruno R. et al. (2015) Experimental analysis of
34 506 thermal interaction between wine cellar and underground. *Energy and Buildings* **104**: 275 - 286.
35
36 507 Tinti, F., Barbaresi, A., Ferrari, M., Elkarmoty, M., Torreggiani, D., et al. (2017a) Experimental
37 508 calibration of underground heat transfer models under a winery building in a rural area.
38 509 *Rudarsko Geolosko Naftni Zbornik* **32(3)**: 15 - 22.
39
40 510 Tinti, F. Barbaresi, A., Torreggiani, D., Brunelli, D., Ferrari, M. et al. (2017b) Evaluation of
41 511 efficiency of hybrid geothermal basket/air heat pump on a case study winery based on
42 512 experimental data. *Energy and Buildings* **151**: 365 - 380.
43
44
45
46
47
48
49
50
51
52
53
54
55
56
57
58
59
60
61
62
63
64
65

1 513 Wu Y., Gan G., Verhoef A., Vidale P. L., Garcia Gonzalez R. (2010) Experimental measurement
2 514 and numerical simulation of horizontal-coupled Slinky Ground Source Heat Exchangers. Applied
3
4 515 Thermal Engineering **30(16)**: 2574 – 2583.
5
6 516 Yalcin T. and Yetemen O. (2009) Local warming of groundwaters caused by the urban heat
7
8 517 island effect in Istanbul, Turkey. Hydrogeology Journal **17(5)**: 1247 - 1255.
9
10 518 Zhao C., Wang Y., Chen X. and Li B. (2005) Simulation of the effects of groundwater level on
11
12 519 vegetation change by combining FEFLOW software. Ecological Modelling **187(2-3)**: 341-351.
13
14 520 Zhu K., Blum P., Ferguson G., Balke K.-D. and Bayer P. (2010) The geothermal potential of
15
16 521 urban heat islands. Environmental Research Letters **5(4)**: pp. 5.

18
19 **522 Figure captions**

20
21 523 *Figure 1. Intervention area (up) and vertical section of the underground cellar, with localization*
22
23 524 *of the three measurement points (down).*

24
25 525 *Figure 2. Mesh of the area chosen for the dynamic simulation.*

26
27 526 *Figure 3: Lithological cross-section for the case study (from Tinti et al., 2017a)*

28
29 527 *Figure 4. Internal temperature of building and cellar*

30
31 528 *Figure 5. Comparison between simulated and estimated temperatures at different depths*

32
33 529 *Figure 6. Comparison between simulated and measured temperature values beside and below*
34
35 530 *the building at measurement points 7 (1.8 m), 8 (2.6 m) and 9 (3.7 m).*

36
37 531 *Figure 7 Simulated area and definition of Section B-B.*

38
39 532 *Figure 8. Section B-B showing ground thermal behaviour affected by the presence of the*
40
41 533 *building and cellar in the characteristic months of January, April, August and October. For each*
42
43 534 *month, the following items are shown: temperature isolines in the ground (black numbers),*
44
45 535 *average temperature in the above ground building and the cellar (red numbers), temperature*
46
47 536 *profile used as boundary condition (black line).*

48
49
50 **537 Table captions**

51
52 538 *Table 1: Key building features.*

53
54 539 *Table 2. Localization of measurement points 7, 8 and 9.*

55
56 540 *Table 3. Entering parameters to estimate ground temperature in the survey area with the*
57
58 541 *analytical method.*

1
2
3
4
5
6
7
8
9
10
11
12
13
14
15
16
17
18
19
20
21
22
23
24
25
26
27
28
29
30
31
32
33
34
35
36
37
38
39
40
41
42
43
44
45
46
47
48
49
50
51
52
53
54
55
56
57
58
59
60
61
62
63
64
65

542 *Table 4. Initial temperature conditions for each layer of the model.*

543 *Table 5. Thermal characteristics associated with the layers.*

544
545 *Table 6. Maximum, minimum and average error of the simulated ground temperature at different*
546 *depths compared to the estimated values by non-linear regression of Equation 1 on*
547 *measurement points (Tinti et al., 2014).*

548 *Table 7. Maximum, minimum and average error of the simulated sensor-based temperature*
549 *compared to the actual values measured.*

Tables

Table 1: Key building features.

	Two-storey building	Wine-ageing room
Width	9.8 m	5.6 m
Length	20.5 m (above ground) + 5.6 m (above cellar)	9.8 m
Height	7.3 m (borders), 8.4 m (centre)	2.6 m (underground)
Walls	25.0 cm thick masonry	25.0 cm thick masonry
Floor	30.0 cm hollow concrete slab	20.0 cm concrete slab
Ceiling	-	30.0 cm hollow concrete slab
Air conditioning	Heating and natural ventilation	Natural ventilation

Table 2. Localization of measurement points 7, 8 and 9.

Sensor number	Depth (m)	Qualitative localization	Orthogonal distance from the building northern wall (m)	Geological layer number (refer to Table 4)
7	1.8	Beside the building and cellar walls	+1.35	6
8	2.6	Under the building, beside the cellar wall	-2.57	7
9	3.7	Under the building, under the cellar	-8.47	9

Table 3. Entering parameters to estimate ground temperature in the survey area with the analytical method.

Yearly ambient temperature (°C)	Yearly amplitude (°C)	Day of minimum temperature (days)	Ground thermal diffusivity (m ² /days)
15.0	15.5	10 th	0.0288

Table 4. Initial temperature conditions for each layer of the model.

Layer n°	Thickness (m)	Depth (m)	Initial temperature (°C)
2	0.25	0.25	4.67
3	0.25	0.50	6.24
4	0.50	1.00	7.80
5	0.50	1.50	10.44
6	0.50	2.00	12.51
7	0.50	2.50	13.47
8	0.50	3.00	14.96
9	1.00	4.00	15.85
10	2.00	6.00	16.45
11	2.00	8.00	16.10

12	2.00	10.00	15.58
13	2.00	12.00	15.52
14	6.00	18.00	15.66
15	7.00	25.00	15.93
16	5.00	30.00	15.37
17	15.00	45.00	15.84
18	5.00	50.00	15.60

Table 5. Thermal characteristics associated with the layers.

Layer n°	Thickness (m)	Depth (m)	Thermal conductivity (W/(m·K))	Volumetric heat capacity (MJ/(m³·K))	Effective porosity (-)
2	0.25	0.25	0.50	1.0	0.1
3	0.25	0.50	0.65	1.5	0.1
4	0.50	1.00	0.65	1.5	0.1
5	0.50	1.50	0.65	1.5	0.1
6	0.50	2.00	0.65	1.5	0.1
7	0.50	2.50	0.65	1.5	0.1
8	0.50	3.00	0.65	1.5	0.1
9	1.00	4.00	0.65	1.5	0.1
10	2.00	6.00	0.65	1.5	0.1
11	2.00	8.00	0.65	1.5	0.1
12	2.00	10.00	0.65	1.5	0.1
13	2.00	12.00	0.65	1.5	0.1
14	6.00	18.00	0.65	1.5	0.1
15	7.00	25.00	1.80	2.4	0.3
16	5.00	30.00	1.00	1.6	0.3
17	15.00	45.00	1.80	2.4	0.3
18	5.00	50.00	2.40	2.4	0.3

Table 6. Maximum, minimum and average error of the simulated ground temperature at different depths compared to the estimated values by non-linear regression of Equation 1 on measurement points (Tinti et al., 2014).

Depth (m)	Maximum Relative Error (%)	Minimum Relative Error (%)	Average Relative Error (%)
0.00	6.1%	0.0%	2.2%
0.25	5.5%	0.0%	2.1%
0.50	5.1%	0.0%	2.3%
1.00	4.7%	0.0%	2.3%
1.50	17.8%	0.1%	9.3%
2.00	13.4%	0.0%	7.3%
2.50	10.3%	0.0%	5.8%
3.00	6.3%	0.0%	3.6%
4.00	4.4%	0.0%	2.5%
6.00	1.9%	0.0%	0.9%
8.00	0.7%	0.0%	0.3%
10.00	0.4%	0.0%	0.2%
12.00	1.5%	1.4%	1.5%
18.00	2.1%	1.9%	2.0%

Table 7. Maximum, minimum and average error of the simulated sensor-based temperature compared to the actual values measured.

Sensor	Depth	Maximum Relative Error	Minimum Relative Error	Average Relative Error
7	1.8 m	19.4%	0.8%	9.0%
8	2.6 m	6.1%	0.1%	2.4%
9	3.7 m	5.3%	0.1%	2.8%

Unpaved road

Ground temperature
campaign area

Wine cellar

Section A-A

Residential building

Winery



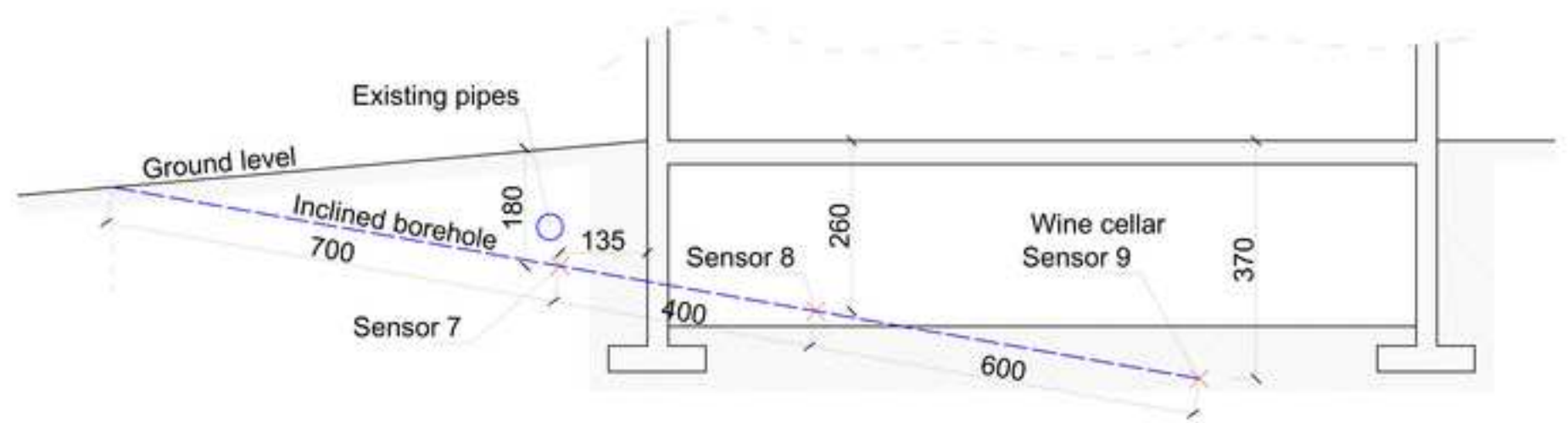
Borehole III

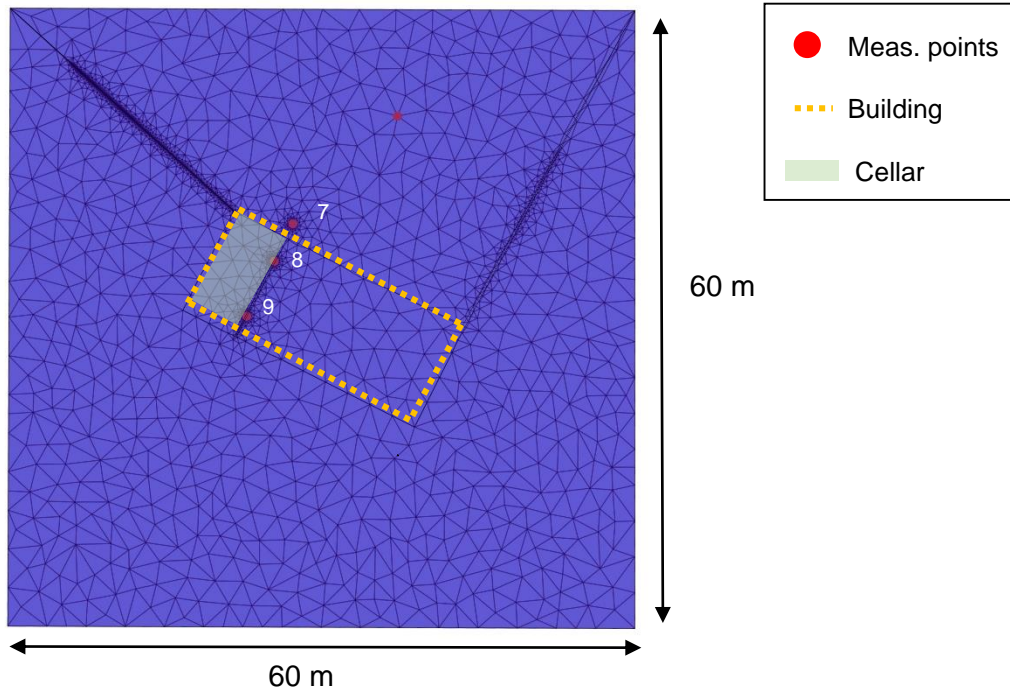
Borehole II

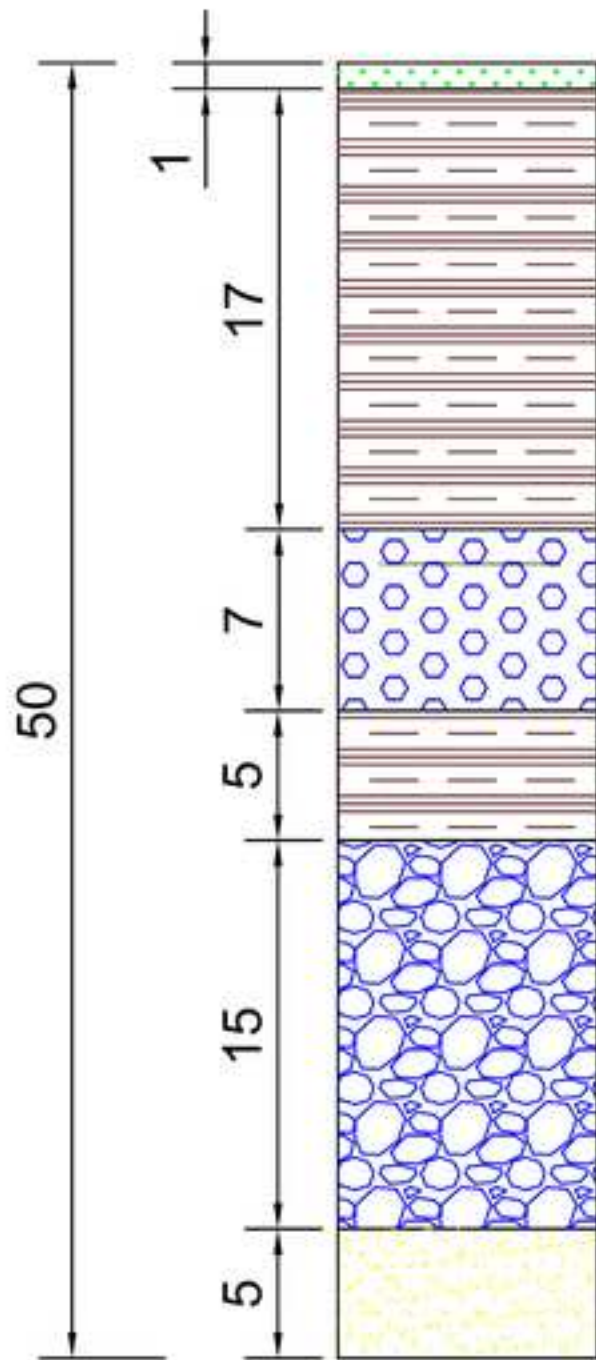
Borehole IV

Borehole I






Section A-A

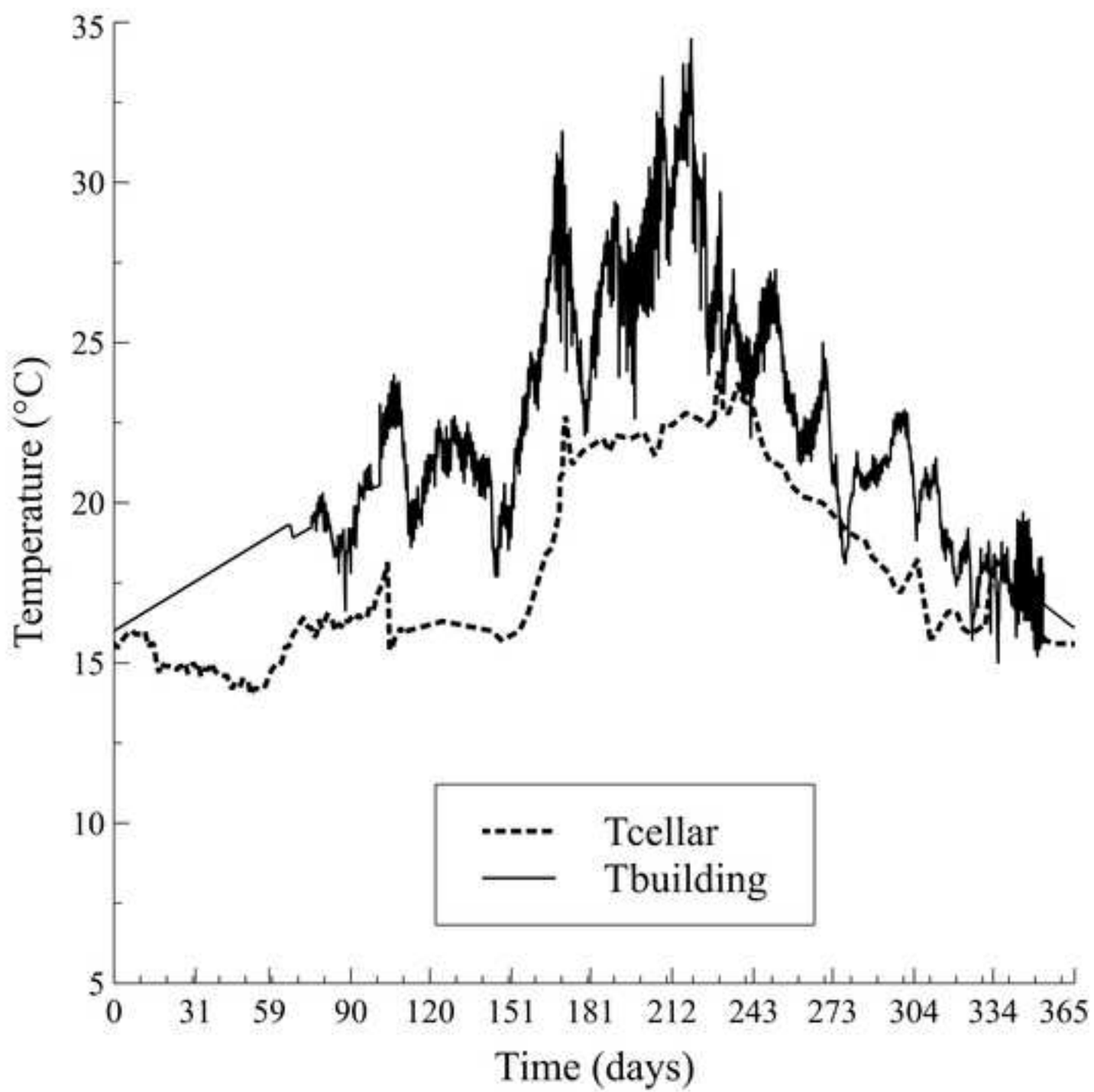


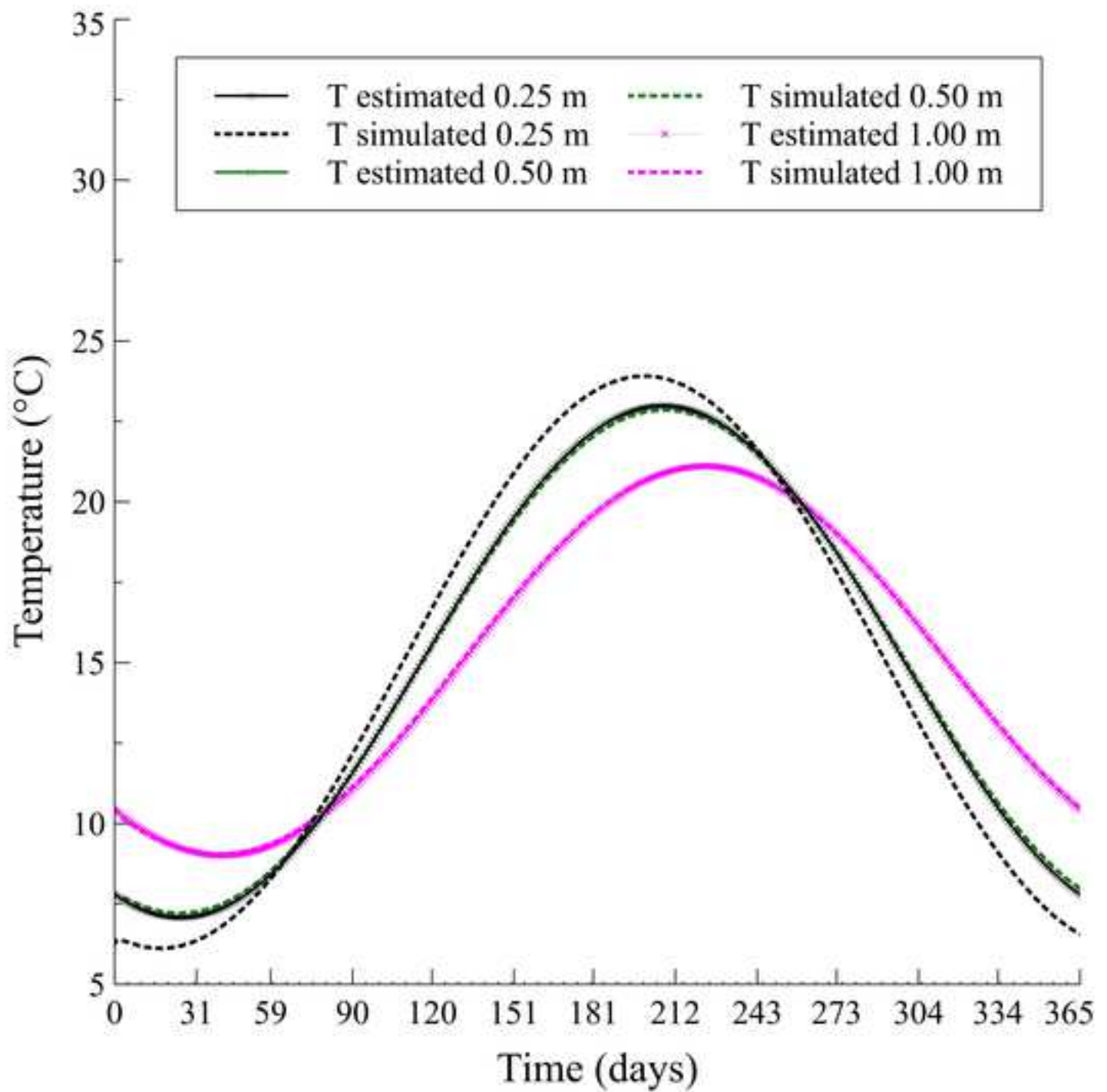


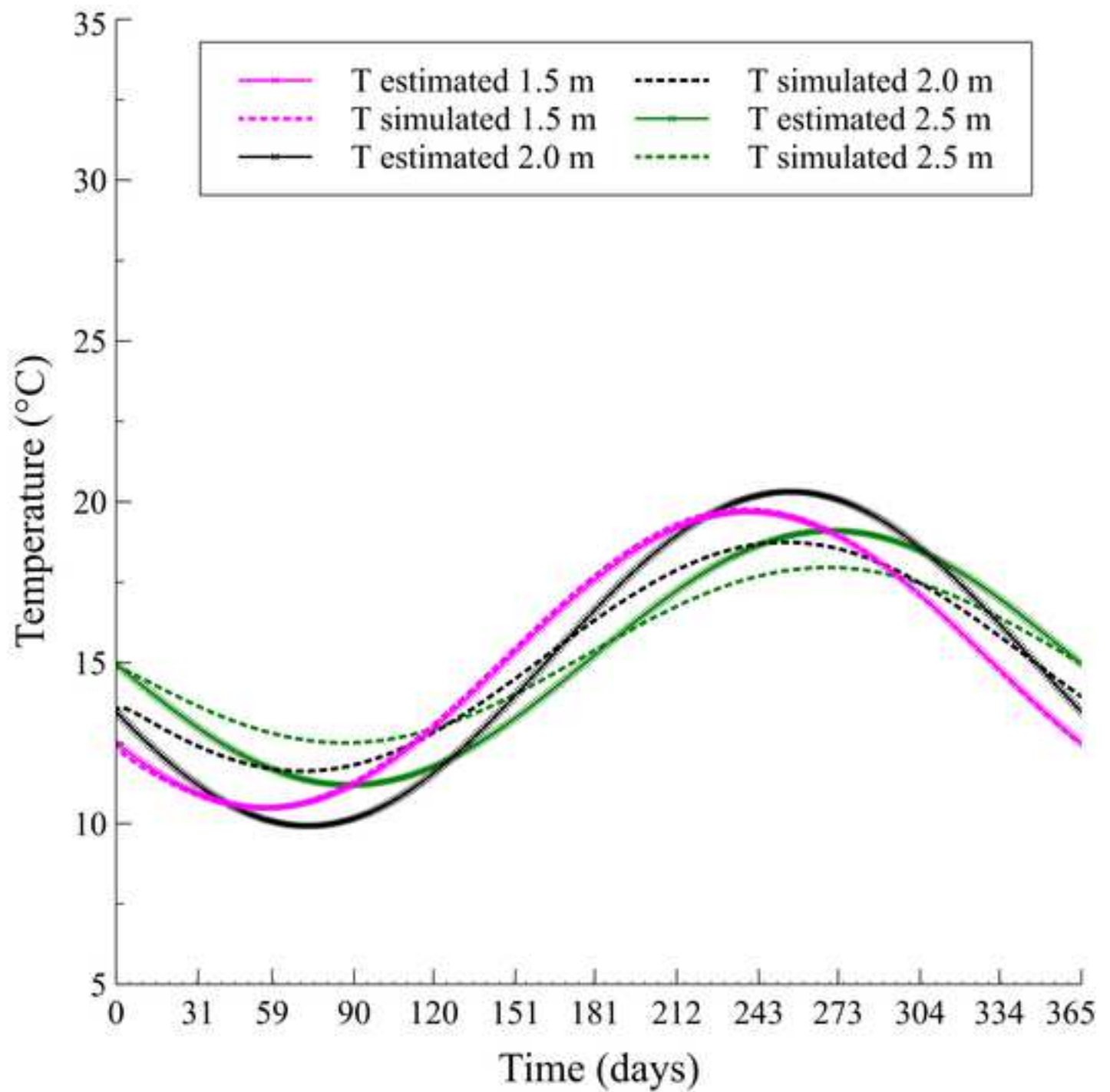


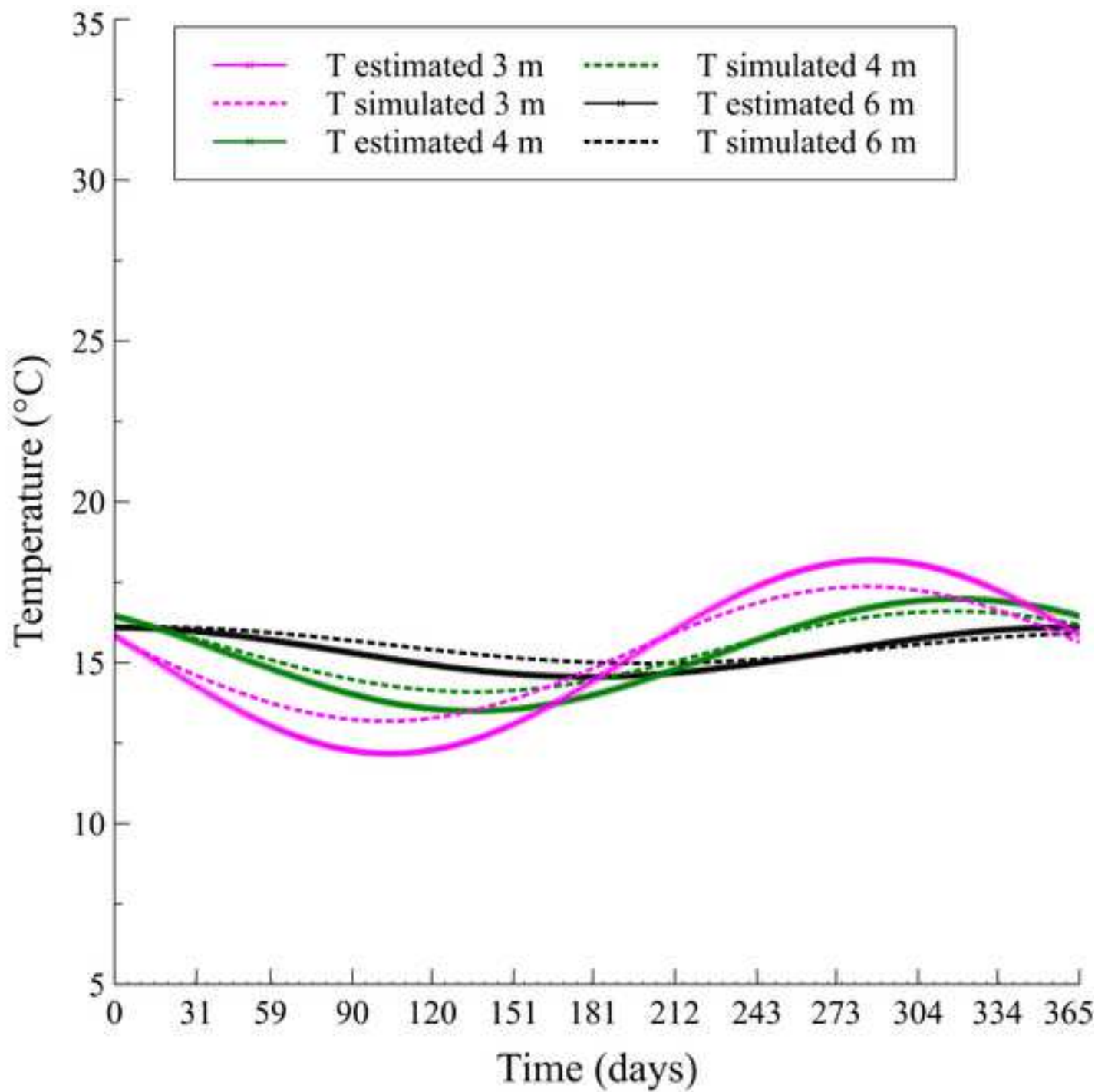
Lithological cross-section
(metric units)

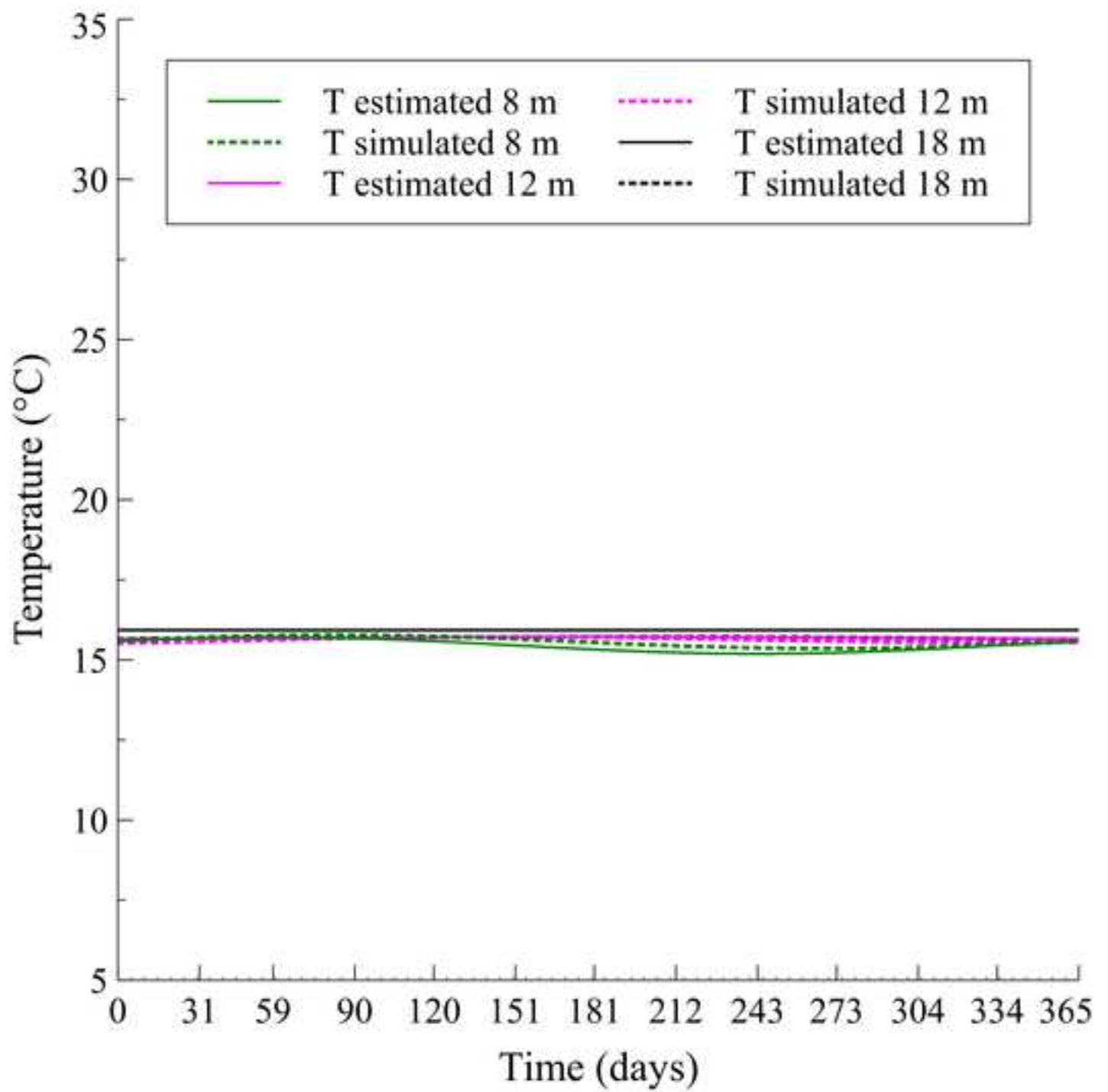
-  topsoil
-  clay
-  unconfined aquifer (gravel)
-  confined aquifer (gravel)
-  sand

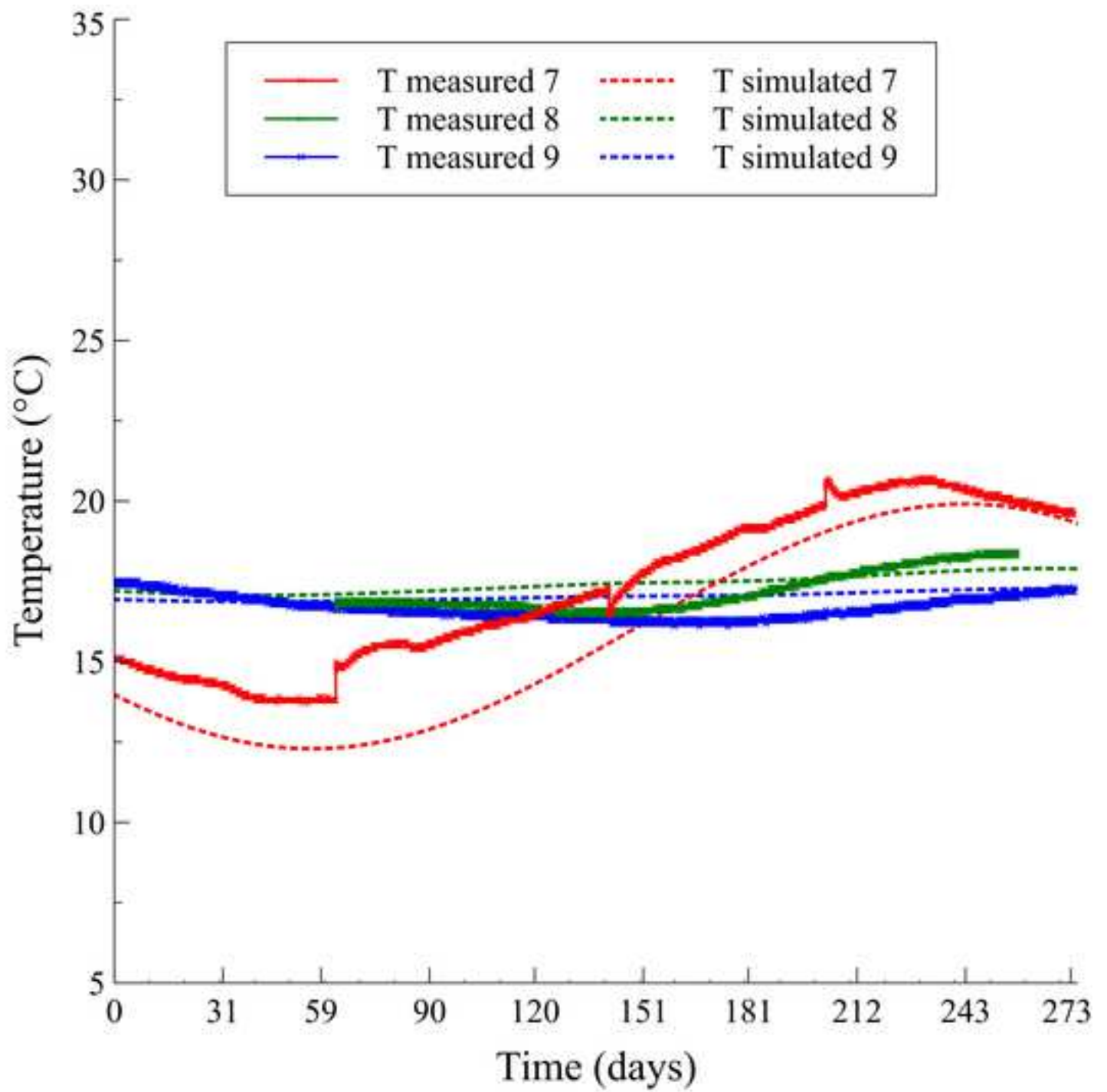


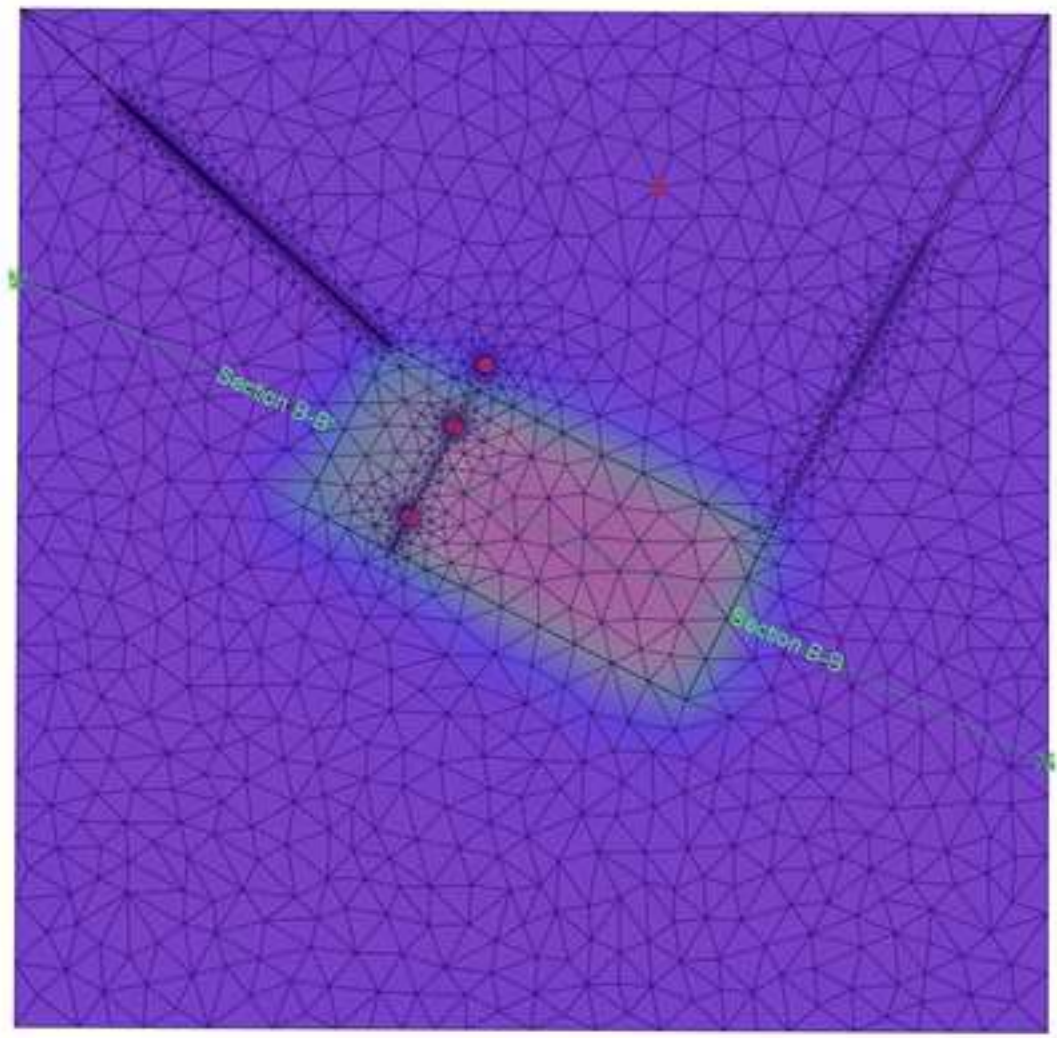






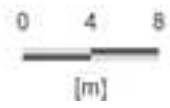


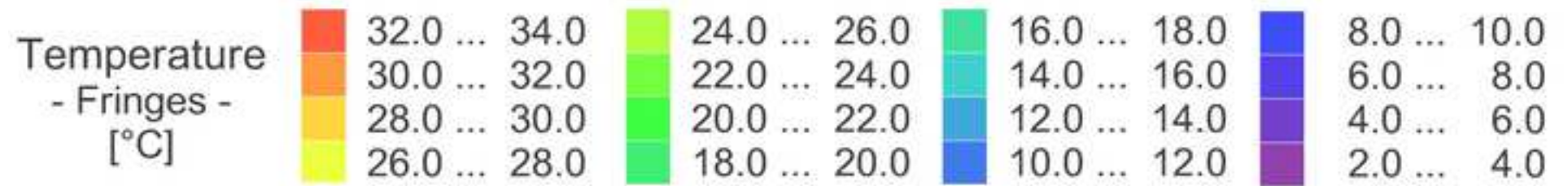


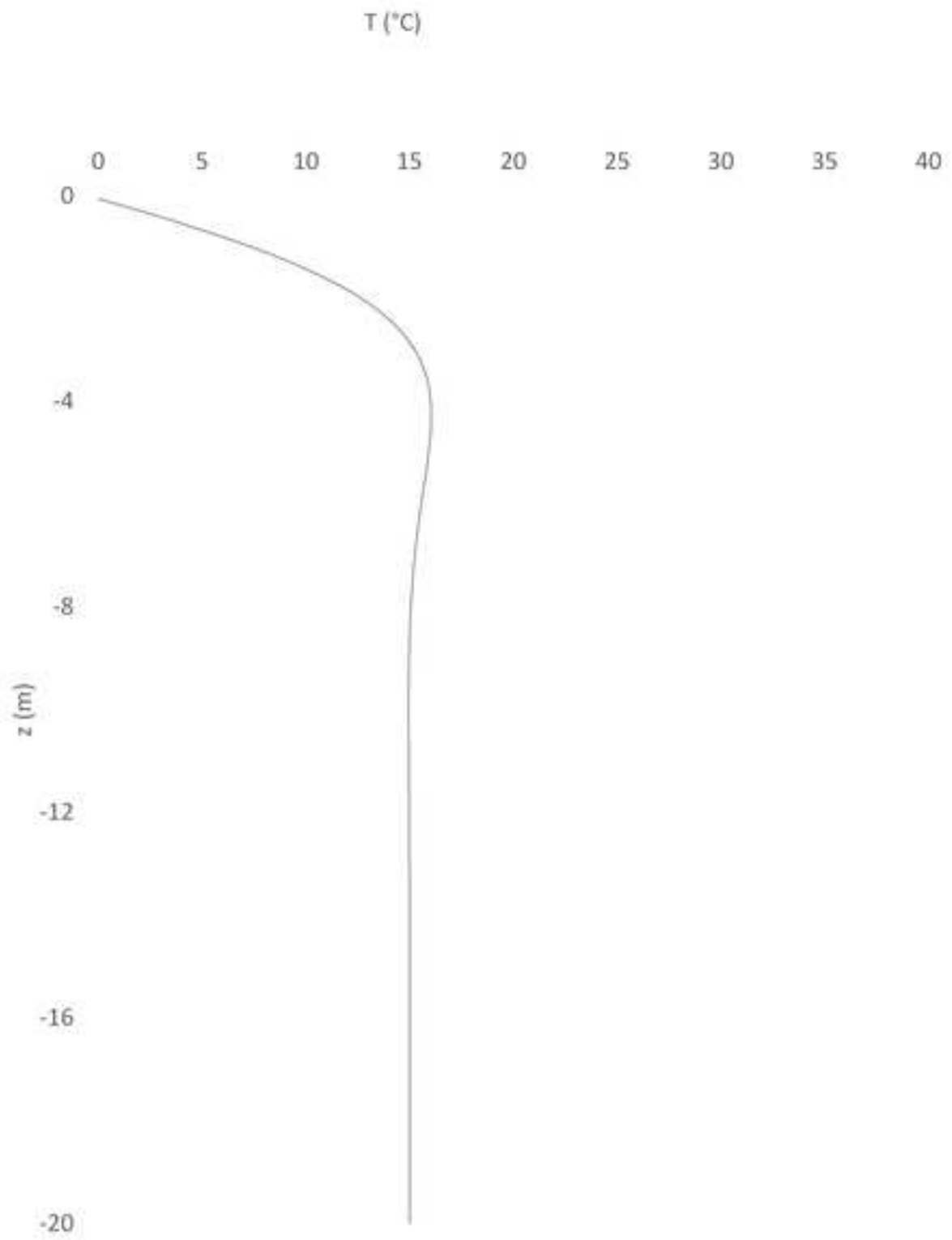


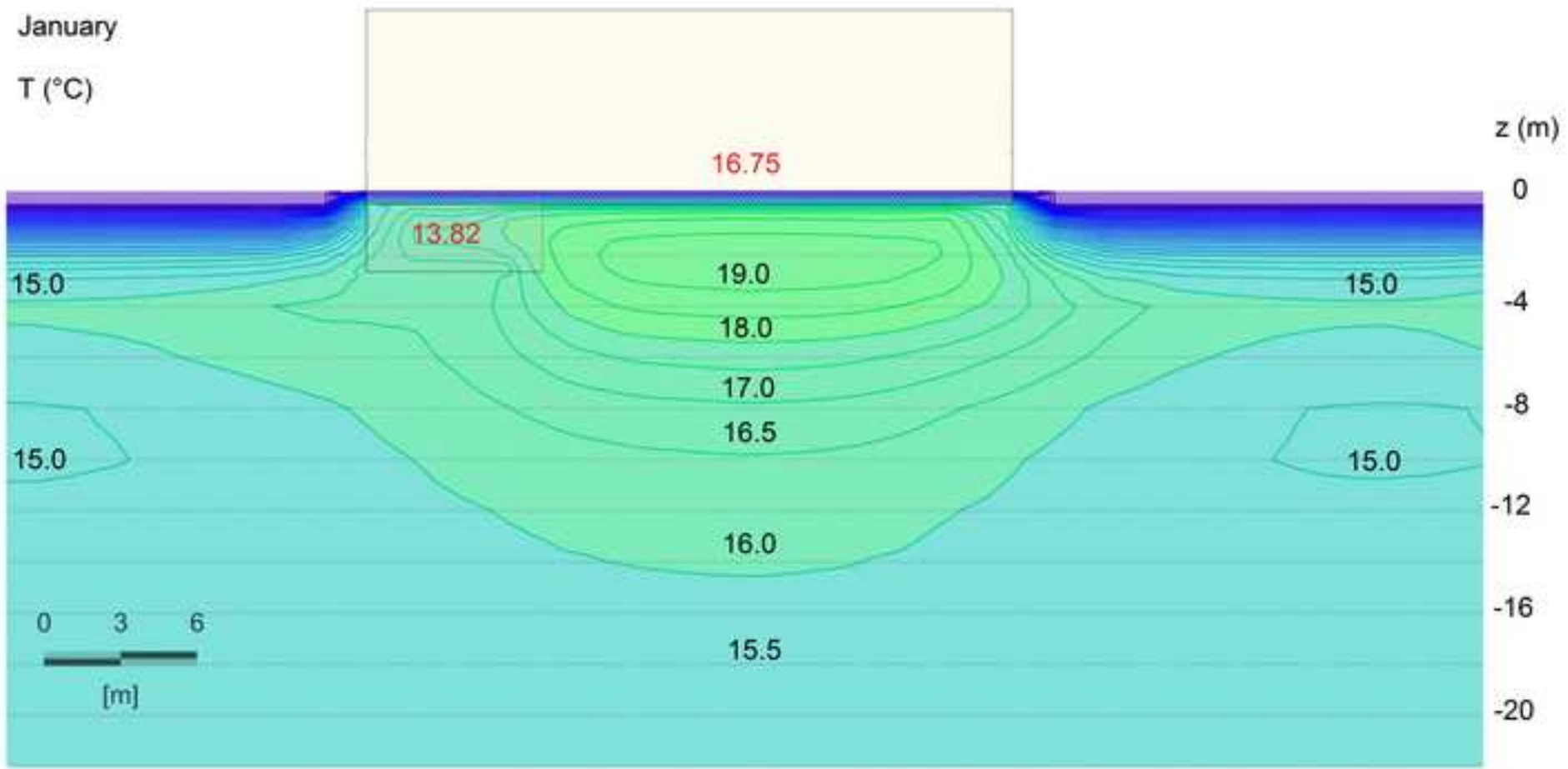
FEFLOW (R)

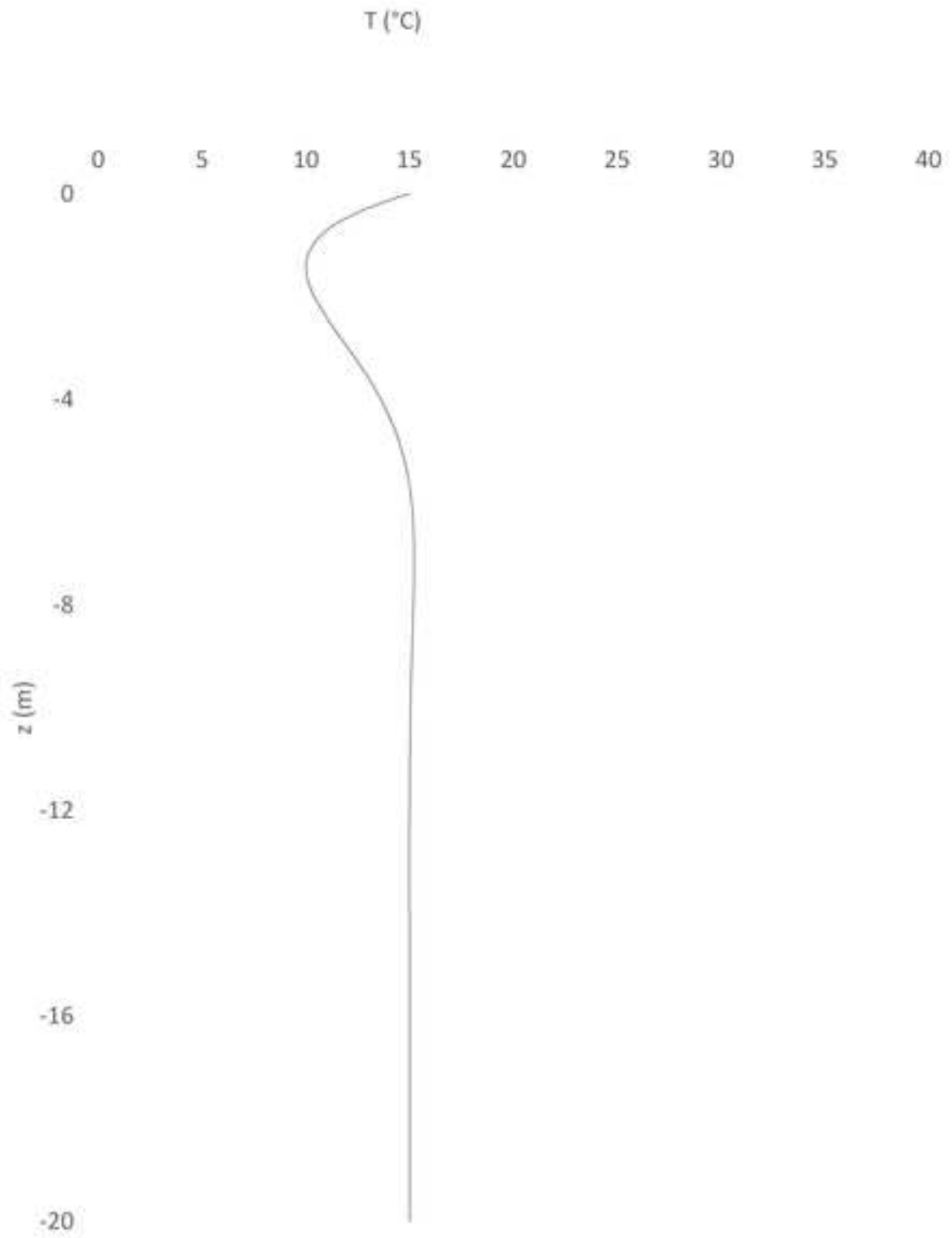
1825 [d]

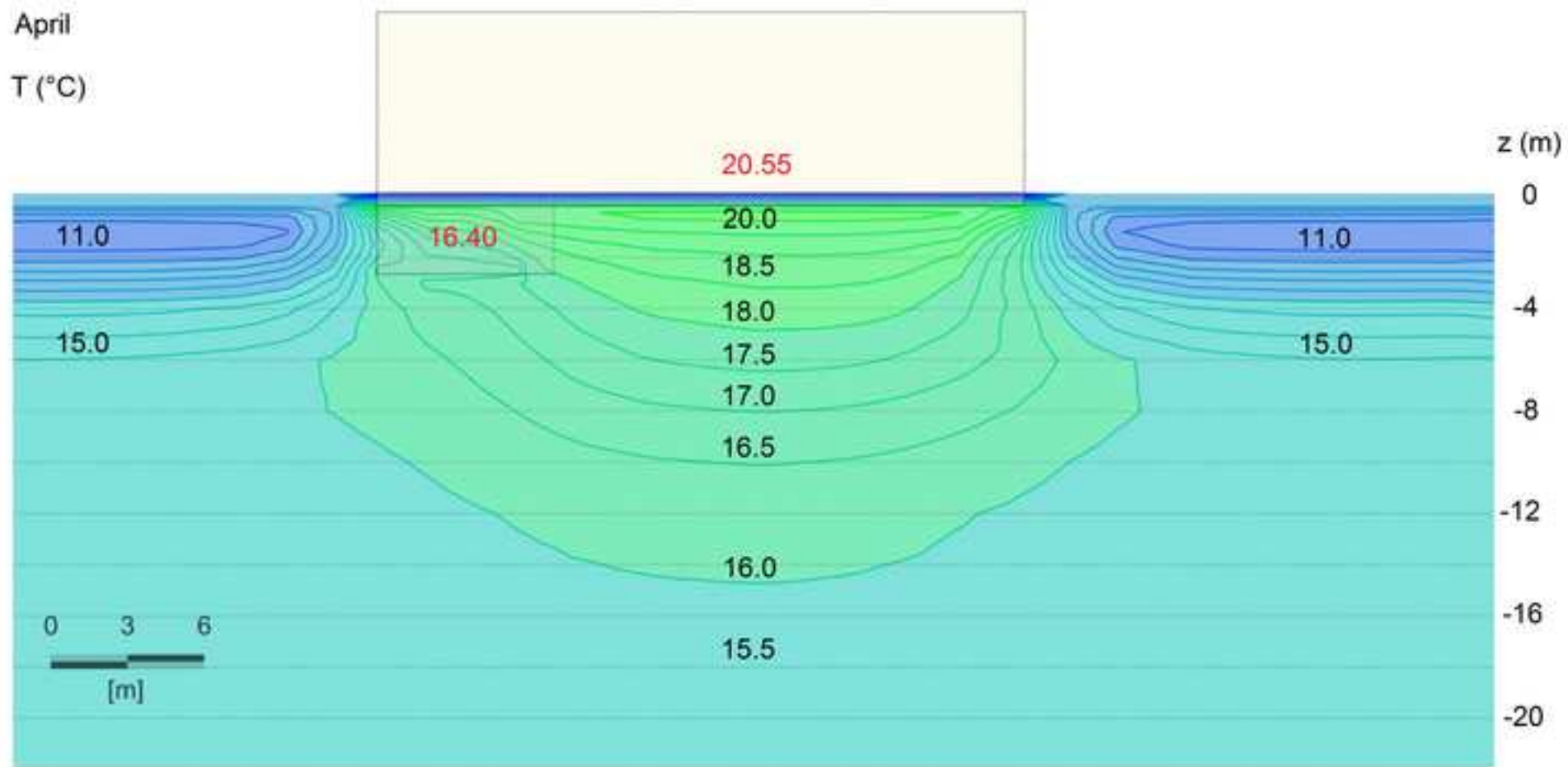


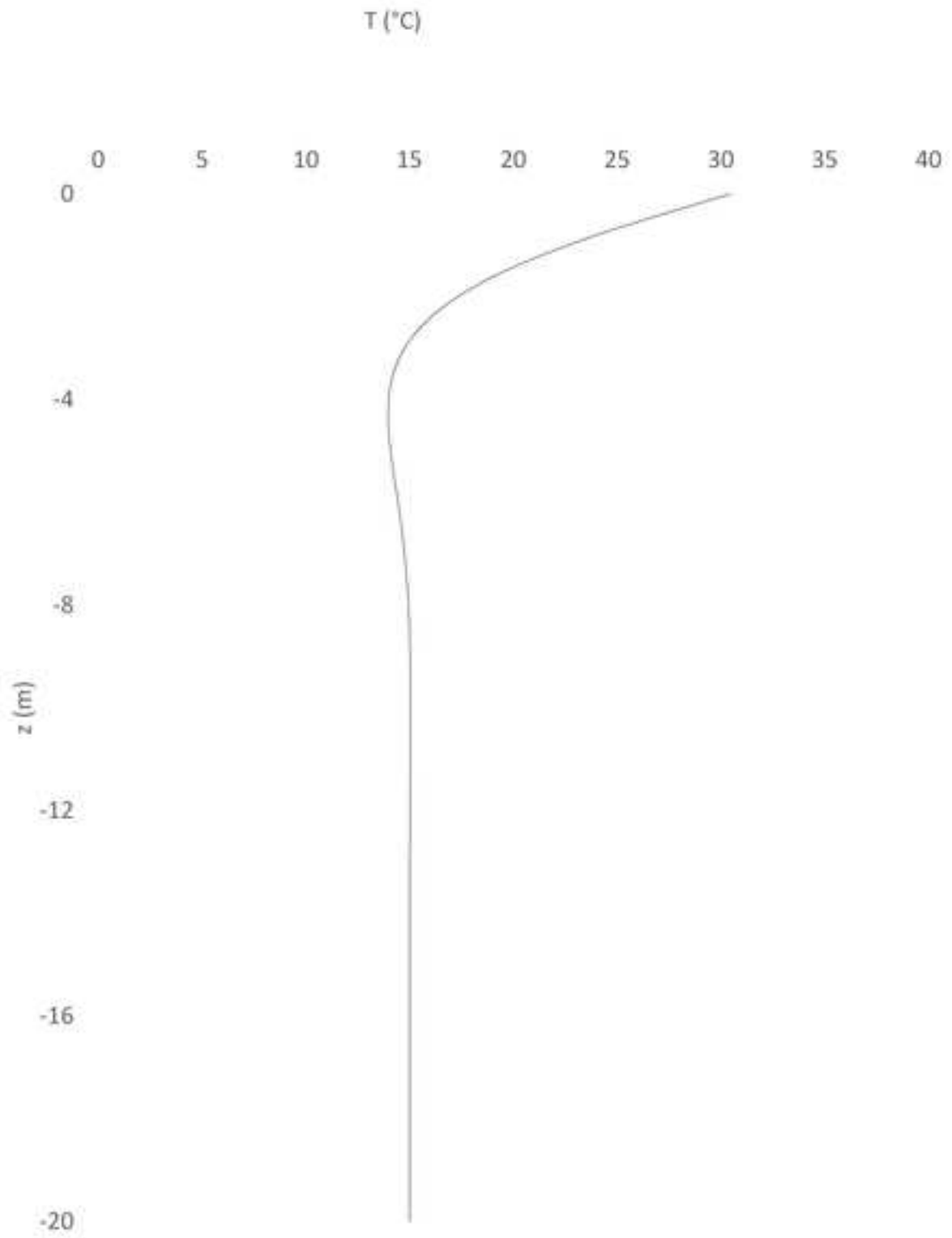


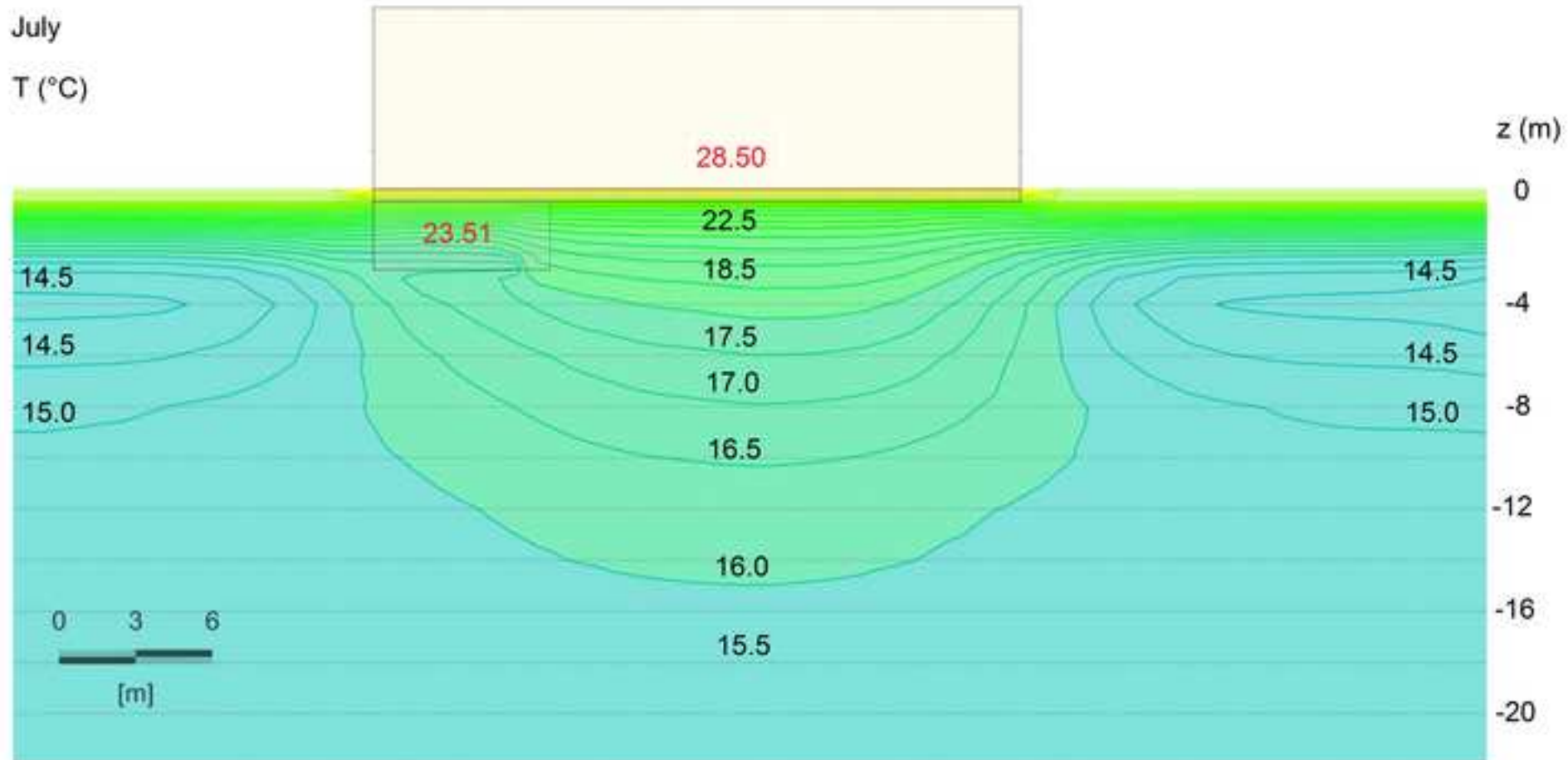


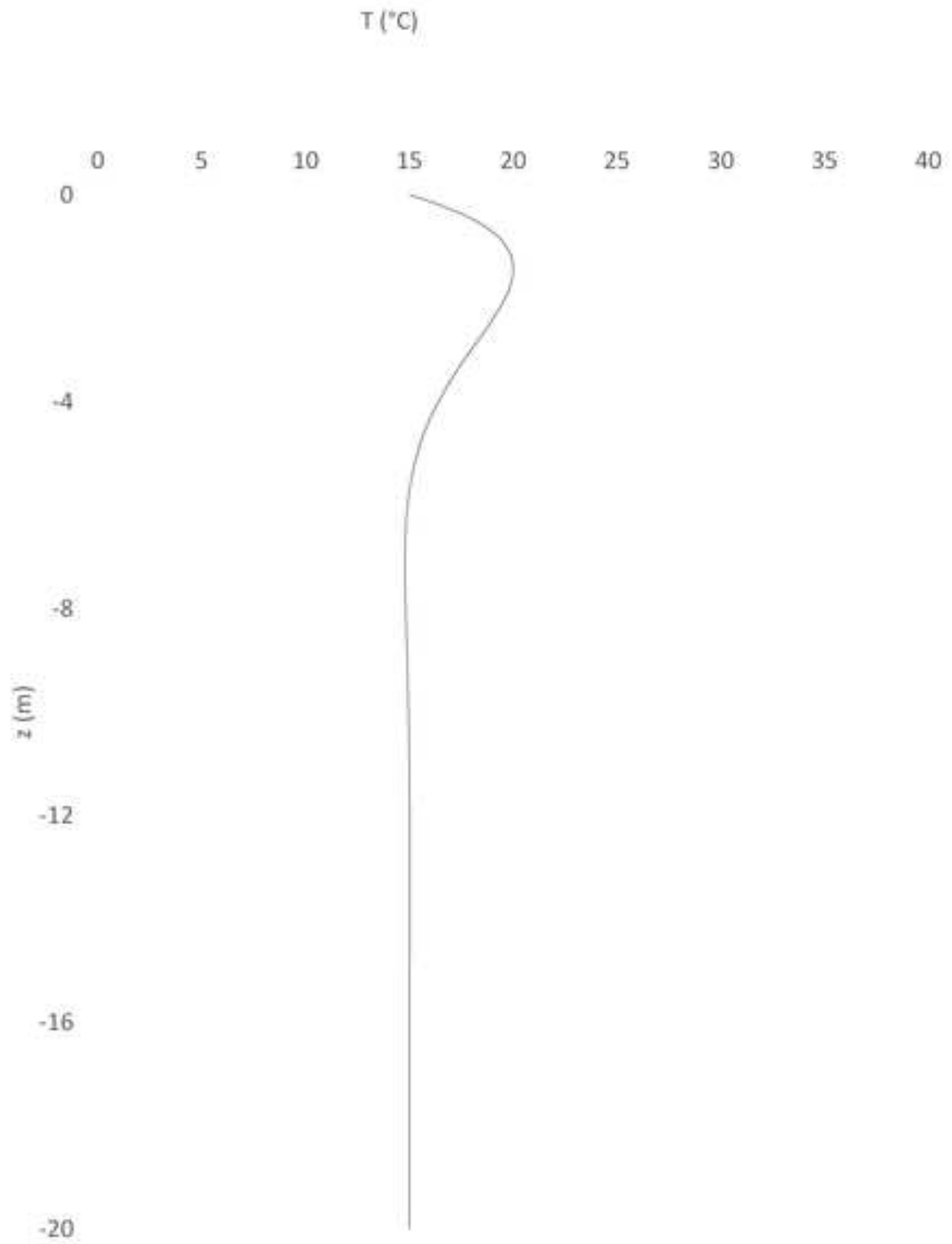












October

T (°C)

